Title

Timescales of storage and recycling of crystal mush at Krafla Volcano, Iceland

Journal

Contributions to Mineralogy and Petrology, 171(6)

ISSN

0010-7999

Authors

Cooper, Kari M
Sims, Kenneth WW
Eiler, John M
et al.

Publication Date

2016-06-01

DOI

10.1007/s00410-016-1267-3

Peer reviewed

Time scales of storage and recycling of crystal mush at Krafla Volcano, Iceland

Kari M. Cooper[1], Kenneth W.W. Sims[2], John M. Eiler[3], Neil Banerjee[4]
[1]Department of Earth and Planetary Sciences, University of California, Davis, One Shields Avenue, Davis, CA 95616. Phone: +1 530-754-8826; fax: +1 530-752-0951.
kmcooper@ucdavis.edu
[2]Department of Geology and Geophysics, University of Wyoming, Laramie, WY 82701
[3]Division of Geological and Planetary Sciences, California Institute of Technology, Pasadena, CA 91125
[4]Department of Earth Sciences, Western University, London, ON N6A 5B7, CANADA

keywords: Iceland; crystal mush; uranium-series disequilibria; oxygen isotopes; magmatic time scales

Abstract

Processes in upper-crustal magma reservoirs such as recharge, magma mixing, recycling of previously-crystallized material, and eruption, affect both the physical state and the chemical composition of magmas. A growing body of evidence shows that crystals in intermediate to silicic volcanic rocks preserve records of these processes that may be obscured due to mixing in the liquid fraction of magmas. Fewer studies have focused on crystals in basaltic lavas, but these show evidence for a more subtle, but still rich record of magmatic processes. We present new ^{238}U-^{230}Th-^{226}Ra data for plagioclase, combined with $\delta^{18}O$ and trace-element measurements of the same crystal populations, from basalts erupted at Krafla Volcanic Center, Iceland. These data document the presence of multiple crystal populations within each sample, with chemical and oxygen-isotope heterogeneity at a variety of scales: within individual crystals, between crystals in a given population, between crystal populations within the same sample, and between crystals in lavas erupted from different vents during the same eruption. Comparison to whole-rock or groundmass data shows that the majority of macroscopic crystals are not in trace-element or oxygen-isotope equilibrium with their host liquids. The most likely explanation for these data is that the macroscopic crystals originated within a highly heterogeneous crystal mush in the shallow magma reservoir system. U-series and diffusion data indicate that the crystals (and therefore the mush) formed recently (likely within a few thousand years of eruption, and with a maximum age of 8-9 ka), and that the crystals resided in their host magma prior to eruption for decades to a few centuries at most. These data, in conjunction with other recent studies, suggest a model where erupted Icelandic magmas are the result of interaction of diverse magmas entering the crust, followed by complex interactions between melts and previously-crystallized material at all crustal levels.

1. Introduction

Processes acting within crustal magma reservoirs affect both the physical state and the chemical composition of magmas within them. For example, magma mixing or recycling of remnant material between sequential eruptions, and cycling between crystals in a mush and a

largely-liquid magma can affect both the chemical compositions of erupted magmas and the compositions of unerupted portions of the reservoir (e.g., Cashman and Blundy 2013), which then can interact with subsequent batches of magma and/or freeze to produce plutonic rocks. Injection of recharge magmas into extant reservoirs add both heat and mass to the system, and can trigger mixing of injected with resident magma (Burgisser and Bergantz 2011; Clynne 1999; Eichelberger 1978), extraction of melt from a largely-crystalline part of the reservoir, and potentially eruptions (Druitt, et al. 2012; Kent, et al. 2010). Conversely, eruptions remove both mass and heat from the system, and the balance of eruption and injection largely controls whether a magma body will grow or stall and freeze (e.g., Degruyter and Huber 2014). Thus, understanding the history of magma mixing and recycling of previously-crystallized material within a magma reservoir is an important component to understanding magma reservoir dynamics and chemical evolution.

Much of the history of magma bodies is obscured in the melt phase due to the relative efficiency of mixing and the averaging of composition between multiple injections of magma. However, crystals contained within volcanic rocks can preserve a unique record of processes such as magma mixing, crystallization, and storage. Many instances of complex crystal cargoes in volcanic rocks have been documented, where features such as major- or trace-element zoning in crystals, isotopic contrasts between crystals and liquids, protracted crystallization ages of crystals, and disequilibrium textures provide strong evidence for differing histories of different mineral and melt phases within a magma (e.g., Bindeman, et al. 2012; Bindeman, et al. 2006; Blundy and Cashman 2008; Cashman and Blundy 2013; Cooper and Kent 2014; Cooper and Reid 2008; Costa, et al. 2013; Costa, et al. 2008; Davidson, et al. 2005; Garrison, et al. 2012; Kilgour, et al. 2013; Marsh 1998; Pyle, et al. 1988; Schmitt 2011; Sims, et al. 2007; Sims, et al. 2013b; Turner, et al. 2003; Zellmer, et al. 2011). This evidence, most frequently documented in the case of arc volcanoes, points to processes such as mixing of multiple phyric magmas, interaction of liquids with resident crystal mush zones, or recycling of remnant material from previous eruptions that are important in producing the spectrum of erupted compositions from a given volcano. Evidence for such complex interactions between crystals, magma mush, and melt is less obvious in oceanic island or midocean ridge settings, where there is often more limited compositional contrast between erupted magmas, but other studies have also suggested such recycling in midocean ridges (Costa, et al. 2010; Feineman and DePaolo 2003; Saal and Van

Orman 2004; Van Orman, et al. 2006; Zellmer, et al. 2011), Hawaii (Clague 1987; Helz 1987; Wright 1973) and Iceland. In the case of Iceland, recent work has documented abundant (albeit sometimes subtle) evidence for recycling of crystalline material within the magma reservoir, including diverse oxygen isotopic compositions of crystals (Bindeman, et al. 2012; Bindeman, et al. 2006), whole-rock major and trace-element compositional diversity within a given eruption (Passmore, et al. 2012), plagioclase and melt inclusion compositions (Neave, et al. 2013), olivine compositional diversity (Thomson and Maclennan 2013), textural evidence, such as crystal size distributions (CSDs) for multiple magmatic components (Higgins and Roberge 2007), and xenolith compositions related to crystal cargoes (Gurenko and Sobolev 2006).

In addition to identifying the processes that have contributed to the compositional evolution of a given magma body, one of the main challenges to understanding the dynamics of magma reservoir processes is quantifying the time scales of processes such as crystal storage within a mush, and time scales of mixing and storage of mixed magmas prior to eruptions. Time scales are important because placing compositional data within a temporal framework allows consideration of links between mixing and eruption, remobilization of mush, and the time scales of storage of eruptible magmas. In this contribution, we use combined U-series data, trace-element data, textural information, and oxygen isotope data for minerals and host magma for samples from the Krafla Fires eruption (1975-1984) in Iceland in order to identify distinct crystal populations and to constrain the time scales of crystal storage and recycling.

2. Background

Measurements of Uranium-series disequilibria have been applied to understanding melt generation and storage in Iceland for decades (Bindeman, et al. 2012; Bindeman, et al. 2006; Condomines, et al. 1981; Hemond, et al. 1988b; Kokfelt, et al. 2003; Kokfelt, et al. 2009; Nicholson, et al. 1991; Sigmarsson 1996; Sigmarsson, et al. 1992a; Sigmarsson, et al. 1992b; Sigmarsson, et al. 1991; Sims, et al. 2013a; Zellmer, et al. 2008). Most of the early studies focused on combining ^{238}U-^{230}Th disequilibria with measurements of other isotopic systems (O, Sr, Nd, Pb) in order to examine the role of crustal contamination or assimilation vs. fractional crystallization in producing evolved magmas at Iceland, and the role of contamination vs. mantle heterogeneities in producing the compositional spectrum in Icelandic basalts (Condomines, et al. 1981; Hemond, et al. 1988b; Nicholson, et al. 1991; Sigmarsson, et al. 1992a; Sigmarsson, et al. 1992b; Sigmarsson, et al. 1991). Most of these studies concluded that fractional crystallization

alone is insufficient to explain the variations in melt composition, but that some combination of crustal contamination/assimilation and mantle heterogeneity are both consistent with the data – although an exception is the study of Kokfelt et al. (2009), which concluded that fractional crystallization alone could adequately explain Sr-Nd-Pb compositions and U-Th-Pa-Ra disequilibria in a suite of lavas from the Snaefellsjökull central volcano. Studies of the influence of crustal material on magma compositions are greatly aided in Iceland by its high latitude and therefore low $\delta^{18}O$ of meteoric waters, which leads to very low $\delta^{18}O$ in hydrothermally-altered crustal rocks (e.g., Bindeman, et al. 2006; Nicholson, et al. 1991).

Those studies that have used U-series data to constrain time scales of magma storage (sometimes in conjunction with diffusion data) have generally concluded that storage times are short - decades to at most millennia (Bindeman, et al. 2012; Bindeman, et al. 2006; Sigmarsson 1996; Zellmer, et al. 2008). Of these studies, only two have measured ages of crystals, in one case ages of major phases (Zellmer, et al. 2008) and in another case zircon (Carley, et al. 2011), with the result that major phases appear to be young (less than a few kyr (Zellmer, et al. 2008); also see discussion in (Cooper 2009; Rubin and Zellmer 2009)) whereas zircon in general are older (mostly tens of kyr, Carley et al. (2011)). When coupled with $\delta^{18}O$ measurements, the zircon ages and compositions suggest that zircon crystals originate from pre-existing hydrothermally-altered material in the crust which resides as a crystal mush or cumulate (Bindeman, et al. 2012; Carley, et al. 2011). Measurements of $\delta^{18}O$ in crystals of major phases also suggests an origin through assimilation of pre-existing material (Bindeman, et al. 2006), although these authors favored a model of assimilation of hyaloclastite rather than crystal mush or cumulate. Prior to this study, no work had been done directly combining U-series ages of major phases with $\delta^{18}O$ of the same phases in order to assess the age and origin of the crystals.

We present results for samples erupted during the 1975-1984 Krafla Fires eruption. This was the most recent eruption at Krafla, beginning in December 1975 and lasting until September 1984 (Sæmundsson 1991; Thordarson and Larsen 2007). The magmatic event occurred as a series of rifting events generally accompanied by fissure eruptions, with most of the volume of lava erupted in the latter half of the eruption (1980-84; Sæmundsson 1991; Thordarson and Larsen 2007). Maps of the evolution of the flow field document which lobes were active at various stages of the eruption, providing a guide to sampling locations corresponding to specific eruptive intervals (Sæmundsson 1991). The eruptive fissures crossed the boundary of Krafla

caldera, and the composition of the erupted magmas varied systematically with location, with quartz tholeiites (relatively low MgO) erupted within the caldera, and olivine tholeiites (relatively high MgO) erupted to the north of the caldera (Gronvold, et al. 2008). These distinctions are consistent in all of the eruptive episodes where the fissure crossed the caldera boundary, and the two types of magmas also show distinctions in Pb, Nd, Hf, and Sr isotopic compositions, indicating that different batches of magma were tapped within and outside of the caldera (Gronvold, et al. 2008).

3. Samples and Methods

3.1 Samples and preparation of mineral separates

We present results for five samples of basalt erupted during the 1975-1984 Krafla Fires eruption (Figure 1) that were collected on a field campaign in 2003 by KM Cooper and KWW Sims. These include two quartz tholeiites from the southern part of the Krafla Fires flow field (03KRA01 and 03KRA02) and three olivine basalts from the northern part of the flow field (03KRA03, 03KRA04, 03KRA05). Eruption dates (inferred from location based on mapping of individual events (Sæmundsson 1991)) and latitude and longitude of sample localities are included in Supplementary Table S1, along with major- and trace-element analyses of whole rock and groundmass (see Results). Of these, we chose two samples (03KRA01 and 03KRA03) for detailed analysis, including U-series analyses of plagioclase separates, oxygen-isotope analyses of plagioclase separates, and trace element compositions of plagioclase by laser-ablation ICPMS. These represent samples of the two different lava types (olivine basalt vs. quartz tholeiite) and were erupted only a few months apart (November 1981 – 03KRA01, January-February 1981 – 03KRA03) therefore allowing comparison of essentially coeval samples of different magma types erupting from different parts of the vent system. For these samples, the rocks were coarsely crushed (to ~1 cm) and fragments which appeared altered or oxidized were removed by hand-picking under a binocular microscope. Clean fragments were rinsed in deionized water, dried, crushed further and sieved. Plagioclase separates were prepared using standard magnetic and density methods. Plagioclase was originally sieved into four size fractions: 63-125 microns, 125-250 microns, 250-500 microns, and 500-1000 microns, and splits of each size fraction were taken for oxygen-isotope analysis and for U-series analysis (although some fractions were combined during bulk analysis for U-series elements in order to obtain

enough sample for analysis; see below). Groundmass separates were prepared by hand-picking fragments of macroscopic minerals from crushed whole-rock samples.

3.2 Major and trace element analyses

Small splits of whole-rock, groundmass, and bulk plagioclase separates were taken from the separates prepared for U-series and oxygen-isotope analysis and were prepared for trace-element analysis separately from the splits used for U-series analysis. Dissolution procedures for the trace-element splits (including whole-rock, groundmass, and plagioclase) followed procedures described in detail in Kelley et al. (2003), and avoided HCl and $HCLO_4$ which minimized interferences and aided in keeping Nb and Ta in solution. Trace element analysis of dissolved splits of whole-rock, groundmass, and bulk plagioclase separates were conducted using ICP-MS at Boston University. Additional splits of whole-rock and groundmass samples were prepared for major element analyses using $LiBO_2$ flux-fusions and were analyzed by ICP-AES at Boston University. Analytical procedures for ICP-MS and ICP-AES followed those described in detail in Kelley et al. (2003).

Trace-element analyses of plagioclase *in-situ* were conducted by LA-ICP-MS at UC Davis and Oregon State University on thin sections and thick sections. Plagioclase LA-ICPMS analyses were performed on an Agilent Technologies 7500a quadrupole ICPMS with a New Wave Research Nd: YAG deep UV (213nm) laser ablation system at the University of California-Davis Interdisciplinary Center for Plasma Mass Spectrometry. Elements analyzed included Ca, Rb, Sr, La, Ce, Nd, Sm, Eu, Gd, Dy, Er, Yb, Lu, Pb, and U. Analytical conditions and techniques were similar to those described in Stelten and Cooper (2012), using a 40 μm spot, 75% power, and 10 Hz. USGS BHVO-2g was used as a calibration standard and was analyzed five times before and after analyses of each sample slide. USGS standard BCR-2g was used as a check standard, and agreement between measured and accepted values ranged from 1% to 5% for all elements except Pb (7%). In particular, Ba concentrations of BCR-2g were within 1% of the accepted value. The agreement between measured and accepted values for the check standard provides the best estimate of accuracy and uncertainty of the trace-element measurements for unknowns. Analyses at Oregon State University were conducted using procedures outlined in Kent et al. (2007). External errors based on multiple analyses of a given sample in the same lab during this time were typically <5% for most elements (Sc, Ti, V, Cr, Mn, Co, Ni, Rb, Sr, Y, Zr, Nb, LREE, Er); <10% for Dy, Gd, Yb, Hf, Ta, Pb; and <15% for U and Th (at 2σ). In this

analytical session, external errors for Ba were <6% (2σ).

3.3 Oxygen-isotope analyses

Small splits of each bulk plagioclase separate were taken from the same bulk separates used for U-series analysis (see below). Aliquots of 1-2 mg each were analyzed by laser fluorination at the California Institute of Technology using a 50W CO_2 laser, BrF_5 reagent, and an apparatus for gas purification and conversion of O_2 to CO_2 based on designs by Sharp (1990) and Valley et al. (1995). Oxygen yields were 13.5 +/- 1.0 μmol/mg, typical of yields for laser-fluorination measurements of fresh glasses (e.g., Cooper, et al. 2004; Eiler, et al. 2000). Measurements of $\delta^{18}O$ were made on two separate days. On each day five to seven analyses of garnet standard UWG-2 (Valley, et al. 1995) were made; reproducibility for repeat measurements of each standard on a given day was 0.02‰ on one day and 0.05‰ on the other day (1σ). The mean $\delta^{18}O$ values for the standard was within ~0.27 ‰ of the nominal value on one day and was within 0.01‰ of the nominal value on the other day, based on previous analyses. All data on unknowns collected on a given day were corrected by a constant value equal to the average difference between measured and accepted (5.75‰ for UWG-2) values for the standard measured on that day. Unknown samples were analyzed two to five times on the same day, with an average standard deviation of multiple analyses of the same sample of ±0.13‰ (1σ), significantly larger than the reproducibility for the standard. Where aliquots of samples were analyzed on separate days their averages for each day agreed within 0.4‰. This likely reflects sample heterogeneity; in similar studies from the same lab where aliquots of the same sample were analyzed on multiple days (e.g., Cooper, et al. 2004; Eiler, et al. 2000) reproducibility of replicate analyses was similar to the reproducibility of the standards in this study.

Oxygen isotopic compositions of whole rock samples were determined in the Laboratory for Stable Isotope Science at the University of Western Ontario and are reported in δ-notation relative to VSMOW (Coplen 1996). Oxygen was liberated from silicates by overnight reaction with ClF3 at 550 °C in sealed Ni reaction vessels, following the method of Clayton and Mayeda (1963), as modified by Borthwick and Harmon (1982). The released oxygen was converted to CO2 over a red-hot carbon rod and its oxygen isotopic composition measured using a dual-inlet DeltaPlus XL stable isotope ratio mass-spectrometer. The $\delta^{18}O$ values of an internal laboratory standard quartz, NBS-30 (biotite) and NBS-28 (quartz) were +11.6 ± 0.2‰, +5.1 ± 0.1‰, and +9.6 ± 0.2‰, respectively, which compares well with their accepted values of +11.5‰, +5.1‰,

and +9.6‰. Reported compositions for unknowns were not normalized to a standard. Sample reproducibility was generally better than ±0.2‰.

3.4 Uranium-series analyses

Whole-rock splits and bulk plagioclase separates were anlyzed for U-series concentrations and isotopic compositions at Woods Hole Oceanographic Institute. Dissolution of separates was conducted at University of Washington using HF-HNO_3 microwave digestion procedures as described in Cooper and Donnelly (2008). U, Th, and Ra concentrations were measured by isotope dilution ICPMS (ThermoFisher Element) and Th isotopic compositions were measured using a ThermoFinnigan Neptune multicollector ICPMS, following procedures described in detail elsewhere (Ball, et al. 2008; Sims, et al. 2008a; Sims, et al. 2008b). Reproducibility using these techniques is better than 1% (2σ) for U and Th concentration measurements and isotopic compositions. Accuracy of Ra concentration measurements for whole-rock analyses was limited by the precision of the NIST 4967 ^{226}Ra standard used for calibrating the spike (1.2% 2σ). Because of the small sample sizes, in-run precision of Ra measurements for plagioclase separates ranged from 0.25%-2.9% (2σ). When propagated with the uncertainty on calibration of the ^{228}Ra tracer solution (1.6% (2σ), which includes spike calibration measurement uncertainties and an uncertainty of 1.2% (2σ) on the concentration of ^{226}Ra in the NIST SRM-4967 solution used to calibrate the tracer solution), this results in an overall uncertainty on Ra concentration measurements of 1.6-4.2% (2σ), as reported in Table 2. Decay constants used in calculating activities are: $\lambda_{232} = 4.9475 \times 10^{-11}$ yr^{-1} (Holden 1990), $\lambda_{230} = 9.1706 \times 10^{-6}$ yr^{-1} (Cheng, et al. 2013), $\lambda_{238} = 1.5513 \times 10^{-10}$ yr^{-1} (Jaffey, et al. 1971), and $\lambda_{226} = 4.332 \times 10^{-4}$ yr^{-1} (Holden 1990).

4. Results

4.1 Textural observations and feldspar populations

Both samples studied in detail (03KRA03 and 03KRA01) contain olivine and plagioclase as phenocryst (i.e. macroscopically visible) phases, and 03KRA01 also contains phenocrystic clinopyroxene. We focused our textural observations on plagioclase in order to provide a context for interpreting the trace-element, oxygen-isotope, and U-series results for plagioclase. Textural observations in thin section and BSE images document multiple plagioclase populations in each

of the two samples; these textural distinctions are supported by compositional variations between populations as discussed in subsequent sections.

The largest feldspar population in Sample 03KRA01 (Population 01-1) consists of blocky crystals, up to several mm in length by ~100-400 microns wide, often present in clusters with other plagioclase crystals (but not other phases). Population 01-1 plagioclase crystals show complex internal zoning, evident in thin section and in backscattered-electron images (Fig. 2a). Clusters of grains show rounding and resorption features that cut across grain boundaries, indicating that the clusters formed prior to resorption (Fig 2a, b). The zoning evident in BSE suggests that these crystals have a wide compositional variation, which is supported by electron-microprobe and LA-ICPMS analyses (see below). A second plagioclase population in sample 03KRA01 (Population 01-2) is present as large, elongate crystals, 2-4 mm long by 300-500 μm wide (Fig 2d). Unlike Population 01-1, these crystals are typically isolated rather than forming clusters. They contain abundant inclusions (primarily melt) and also show evidence for resorption. Groundmass plagioclase grains are present as laths ~100 x 15-20 μm.

Sample 03KRA03 also contains two phenocrystic feldspar populations. Population 03-1 consists of large blocky crystals mostly 200-500 μm long but occasionally up to several mm in length that often are located in clusters (Fig 2e. As with Population 01-1, there is evidence for resorption that cross-cuts grain boundaries within the cluster, indicating that resorption occurred after the cluster was formed. A second population of plagioclase is present (Population 03-2), primarily as elongated, isolated crystals, some very large (~200-700 μm long by 75-475 μm wide) (Fig 2f), but occasionally occurring in radial clusters with plagioclase and other phases. Some population 03-2 crystals show complex internal zoning including apparent dissolution surfaces (Fig 2f). Groundmass plagioclase crystals are present as laths on order of 50-100 microns long by 10-30 microns wide.

4.1 Major and trace-element data

4.1.1 Whole-rock analyses

Whole-rock and groundmass major and trace-element data are presented in Supplementary Table S1. Samples 03KRA01 and 03KRA02 are moderately evolved quartz tholeiites (SiO_2 49.7-50.5 wt%; MgO 5.80-5.86 wt%). 03KRA01 groundmass has slightly higher MgO and lower SiO_2 than the whole-rock (5.99 wt% and 49.75 wt%, respectively), consistent with feldspar being

the dominant phenocryst phase. Samples 03KRA03, 03KRA04, and 03KRA05 are somewhat more primitive olivine basalts (SiO_2 =48.8-49.3 wt%; MgO 7.25-7.55 wt%). Rare-earth element data are presented in Figure 3. All samples studied here show smooth, LREE-enriched patterns that fall within the field of Krafla basalts (downloaded from the GeoRoc database on 9/23/2014; see caption to Fig. 3 for references). The quartz tholeiite samples have higher REE concentrations than do the olivine basalts, consistent with their more evolved major-element compositions. Similarly, groundmass for sample 03KRA01 has slightly higher REE concentrations than the whole rock, consistent with the removal of trace-element depleted phenocryst phases (plagioclase, pyroxene and olivine) from the groundmass separate.

4.1.2 Plagioclase major- and trace-element analyses

Major-element compositions were analyzed *in situ* in thin section by electron microprobe. Individual analyses of plagioclase major-element composition range from ~An_{50}-An_{80} in sample 03KRA01, and ~An_{60}-An_{90} in sample 03KRA03 (Fig. 4, Supplementary Table S2). The most albitic plagioclase is present in Population 01-2 (~An_{50}), distinct from other plagioclase populations in the two samples. There is significant compositional overlap between Populations 01-1 and 03-2 (between An_{60} and An_{80}), but Population 03-1 has higher An (~An_{80}) and Population 01-2 has lower An (~An_{50}). Groundmass plagioclase crystals in Sample 03KRA03 yielded compositions of ~An_{70} (Supplementary Table S2). No groundmass crystals were analyzed in sample 03KRA01.

Plagioclase trace-element compositions were analyzed both in the bulk separates (splits of the dissolved separates used for U-series analyses) and *in situ* by LA-ICPMS. All analyses of plagioclase have lower concentrations of rare-earth elements than do the corresponding groundmass or whole rock analyses (with the exception of Eu in one plagioclase population; Figure 3), as expected based on the strongly incompatible nature of all rare-earth elements but Eu in feldspar and the relative compatibility of Eu (e.g., Bindeman and Davis (2000)). Data for the bulk mineral separates show that the large size fraction of plagioclase from 03KRA03 has significantly lower concentrations of rare-earth elements than does the small size fraction, and the slope of the rare-earth element pattern is steeper for the large size fraction than the smaller size fraction (Fig 3b). Similarly, the slope of the rare-earth element pattern is shallower for the small size fraction of plagioclase than for the large size fraction from 03KRA01, although absolute concentrations are more similar to each other than for the two size fractions in sample

03KRA03, resulting in crossing rare-earth element patterns for sample 03KRA01 (Fig 3b). Laser-ablation data for plagioclase is also shown on Figure 3b, presented as averages of multiple individual analyses of crystals in the different populations. The heavy REE were below detection limits for the quadrupole laser-ablation system, and thus are not shown on the diagram. However, comparison of LREE data for in-situ and bulk analyses of plagioclase show broad agreement of the laser and bulk separate data, considering the larger uncertainties in the laser-ablation data.

Other trace elements in plagioclase, which can be measured to higher precision (e.g. Ba, Figure 4), allow a more robust comparison of the trace-element composition of the different plagioclase populations. For example, the combined An-Ba data show that Population 01-2 is compositionally distinct from other populations (although it should be noted that only two of these large elongate crystals were present in the analyzed thin sections, so the full compositional range of this population may be greater than what is shown). There is broad overlap in the An content and Ba concentrations of Populations 01-1 and 03-2, but Population 03-2 extends to higher An than does Populations 01-1. Population 03-1 has the highest An of the populations. Compositional diversity is also evident at the scale of single crystals – data for two crystals from Population 01-1 are highlighted in Figure 4, showing significant compositional changes within individual crystals. Finally, the majority of analyses are not consistent with equilibrium crystallization from the host liquid at 1000-1200 °C, based on calculated and experimentally-derived partition coefficients (Figure 4) (Blundy and Wood 2003a; Blundy and Wood 2003b; Fabbrizio, et al. 2009).

4.2 Oxygen-isotope analyses

Oxygen-isotope data for whole rock samples and plagioclase separates are summarized in Table 1 and Figure 5. Whole-rock $\delta^{18}O$ for 03KRA01 and 03KRA03 is 5.08 ‰ and 4.62 ‰ respectively. These samples are somewhat higher in $\delta^{18}O$ than other Krafla samples with similar MgO contents (Nicholson, et al. 1991), although the other Krafla data do show a significant scatter. Multiple analyses (2-5) of small aliquots of plagioclase from three different size fractions of each sample are also shown on Figure 5. The different analyses of each size fraction scatter more broadly than can be explained by the reproducibility of the measurements (as assessed by replicate analyses of homogeneous samples at Caltech), with the exception of the three replicates of the 250-500 micron size fraction for 03KRA01, indicating oxygen-isotope heterogeneity

within the bulk separates for most of the size fractions. The average $\delta^{18}O$ for each size fraction is different for plagioclase in 03KRA01 compared to the same size fraction in 03KRA03, although there is overlap between analyses of some of the individual aliquots. In addition, the data for 03KRA03 show a decrease in average $\delta^{18}O$ with increasing size fraction suggesting that, at least for 03KRA03, the larger size fractions dominantly sample a different plagioclase population than do the smaller size fractions. The same pattern is suggested by the averages for each size fraction for 03KRA01, although the standard deviation of the individual replicates for 03KRA01 is large enough that the averages of small and large size fractions are within two standard deviations of each other. Finally, none of the individual analyses are within the range expected for crystallization from their respective host liquids, assuming $\Delta_{plag\text{-}melt}$ of 0-0.4 ‰ (following Eiler (2005) and Bindeman et al. (2006); calculated by combining $\Delta_{plag\text{-}olivine}$ of ~0.6-1.1‰ for equilibrium between forsterite and $An_{50\text{-}100}$ plagioclase at temperatures of 1150-1350°C and equilibrium $\Delta_{basalt\ melt\text{-}olivine}$ of ~0.5‰ (Bindeman, et al. 2006; Chiba, et al. 1989; Eiler 2001; Eiler, et al. 2005)).

4.3 Uranium-series analyses

Uranium-series data for whole rock, groundmass, and plagioclase separates are presented in Table 2 and Figure 6. Concentrations of U, Th, Ra and Ba for whole rock and groundmass are within the range of data from previous U-series studies of Icelandic basalts (Condomines, et al. 1981; Hemond, et al. 1988a; Kokfelt, et al. 2003; Kokfelt, et al. 2009; Koornneef, et al. 2012a; Sigmarsson 1996; Sigmarsson, et al. 1992a; Sigmarsson, et al. 1992b; Sigmarsson, et al. 1991; Zellmer, et al. 2008). Concentrations of Th, U and Ba in plagioclase separates for this study are somewhat higher than the plagioclase separate from Veidivötn (located in south-central Iceland) basalt T2 analyzed by Zellmer et al. (2008) (e.g., Th concentrations in plagioclase separates of 44-73 ppb in this study compared to 37 ppb for T2 plagioclase); a direct comparison of Ra data is not possible because no Ra data are available for that sample. In addition, concentrations of U and Th, in plagioclase separates from this study are higher than that predicted by plagioclase-melt partition coefficients (D_U of ~$6x10^{-4}$ and D_{Th} ~5.6 times D_U; Blundy and Wood (2003a)). In addition, U/Th ratios of plagioclase are higher than predicted from partitioning behavior. These observations are most simply explained by the presence of small amounts of glass in the mineral separates (either as melt inclusions and/or adhering to the outsides of grains). The difference in

measured and predicted U and Th concentrations is consistent with the presence of up to ~5% glass in the bulk separates. Alternately, the high U and Th and U/Th in plagioclase compared to predictions could indicate that the plagioclase crystallized from melts with higher U and Th concentrations and U/Th ratios than the host liquid. These two explanations are not mutually exclusive.

(^{230}Th)/(^{238}U) ratios of whole rock in this study were 1.13 to 1.25, also similar to other Icelandic basalts and in particular to the Zellmer et al. (2008) T2 and T6 Veidivötn basalt data with (^{230}Th)/(^{238}U) of 1.12-1.14. (^{230}Th)/(^{232}Th) ratios for the whole rock and groundmass samples analyzed in this study were 1.099-1.011, somewhat lower than the T2 and T6 data of 1.061-1.063 (Zellmer, et al. 2008). All plagioclase separates analyzed in this study had (^{230}Th)/(^{232}Th) within error of the whole rock. Taken at face value, the U-Th data for 03KRA01 and 03KRA03 yield 3-point isochron ages of 3.0 +6.1/-6.0 and 2.0 +9.1/-8.5 kyr, respectively, assuming that the plagioclase crystallized from the host liquid (Figure 6a) (ages calculated using IsoPlot v. 3.75, using the Monte Carlo error estimates; Ludwig (2001)). The consequences on calculated ages of assuming a different melt composition are discussed below (section 5.3).

(^{226}Ra)/(^{230}Th) ratios for whole rock samples in this study were both 1.05 (Table 2; Figure 6b), again similar to previous results for Icelandic basalts (Bindeman, et al. 2006; Kokfelt, et al. 2003; Kokfelt, et al. 2009; Sigmarsson 1996; Zellmer, et al. 2008). Analyses of plagioclase show higher ^{226}Ra excesses than whole rocks ((^{226}Ra)/(^{230}Th) of 1.08-1.98), qualitatively consistent with the pattern expected from young crystals based on theoretical and experimental studies of partitioning behavior of Ra (Blundy and Wood 2003a; Fabbrizio, et al. 2009). However, Ra concentrations and Ra/Ba ratios in plagioclase are higher than predicted based on partitioning if the plagioclase crystallized from the host melt (Blundy and Wood 2003a; Fabbrizio, et al. 2009). The implications of this result (including the implications for ^{230}Th-^{226}Ra age calculations) are discussed below.

5. Discussion

5.1: Chemical and isotopic heterogeneity in plagioclase crystal populations

A first-order interpretation emerging from the trace-element and oxygen-isotope data is that each sample of Krafla basalt studied here contains at least two chemically-distinct populations of macroscopic crystals that are not in chemical or isotopic equilibrium with their host liquids.

Furthermore, the crystal populations in the two samples are distinct from each other, despite being erupted essentially coevally from vents spaced within ~10 km of each other. This conclusion is robust despite some ambiguity about comparing the different types of data (for example comparing groups based on textures to groups based on size fraction of mineral separates). For example, the textural populations can be related directly to the *in-situ* trace-element analyses, allowing comparison of the trace-element characteristics of each textural population. However, the multiple size fractions analyzed for oxygen-isotope and U-series data do not correspond directly to the textural populations, considering that there is overlap between crystal sizes between the populations, and because due to crushing and preparation of mineral separates, some fragments of the larger crystals will be incorporated into the smaller size fractions. A diagram comparing the size fractions of separates analyzed for U-series and oxygen-isotope analyses to the crystal sizes analyzed in-situ is shown in Figure 7. As is evident from Figure 7, although there is not a one-to-one correspondence between the sizes of crystals analyzed by each of the different techniques, there is significant overlap between the populations sampled by each technique. Therefore, although a detailed comparison of, for example, $\delta^{18}O$ to Ba concentrations in Population 01-1 is not possible, general patterns in $\delta^{18}O$ and U-series data with crystal size can be related to the general textural observations, and can be compared between the two samples.

For example, the diversity in $\delta^{18}O$ for the different size fractions in each sample indicate that there must be some oxygen-isotope heterogeneity within the crystals in each case. The long dimension of some of the crystals in each of the four textural populations defined here is greater than 250 μm, which means that even the largest size fraction analyzed for oxygen isotopes could have sampled both of the macroscopic textural crystal populations for each of the size fractions. However the largest size fraction analyzed for $\delta^{18}O$ is likely to be dominated by the largest textural population. In that case, the difference in average $\delta^{18}O$ of the largest and smallest size fractions for 03KRA03 likely indicates a difference in average $\delta^{18}O$ of plagioclase populations 03-1 and 03-2. Similarly, the difference in $(^{226}Ra)/(^{230}Th)$ for the two size fractions of plagioclase in 03KRA03 also likely indicates a difference in the U-series characteristics of Populations 03-1 and 03-2 (such a comparison is not possible for 03KRA01 as the radium analysis of the large size fraction failed due to small sample size). Nevertheless, even if there was a sampling bias during crushing such that the size fractions have little to no correspondence with the textural

populations, the observation of oxygen-isotope and U-series heterogeneity between size fractions must indicate that there is isotopic heterogeneity within the crystals at a spatial scale smaller than that of the analyzed aliquants. In the case of the oxygen-isotope analyses, the aliquant size was 1-2 mg, corresponding to a few crystal fragments in the largest (>500 micron) size fraction analyzed. Furthermore, the differences in oxygen-isotope and U-series data between the two samples also indicates a larger spatial scale of compositional heterogeneity, where the crystals sampled by different parts of the fissure at essentially the same time were distinct from each other.

Trace-element heterogeneity is also apparent at a variety of scales. For example, the solution REE data show differences between size fractions within a given sample and between the two samples (Figure 3). The laser-ablation REE analyses can be related more directly to the textural populations than can the oxygen-isotope data; for example, average REE data show some differences between the different textural populations (Figure 3). The *in-situ* Ba analyses of plagioclase most clearly show heterogeneity at a variety of scales: between the different crystal populations (e.g., Population 03-1 vs. 03-2), within a given population (i.e., a significant spread in Ba concentration and An compared to analytical uncertainty within each crystal population), and within single crystals (Figure 4).

The relationship of crystals to host liquids can also be assessed using these data. For example, our oxygen isotope data show that none of the analyzed crystal populations are in isotopic equilibrium with the host liquid (assuming plagioclase-liquid oxygen-isotope fractionation of 0-0.4‰ as described above; Figure 5). This is supported by the fact that the majority of Ba concentrations measured *in situ* are not in chemical equilibrium with the host liquid (Figure 4). Furthermore, none of the size fractions analyzed for U-series disequilibria have (^{226}Ra)/(^{230}Th) consistent with crystallization from their host liquids. A (^{226}Ra)/[Ba] evolution diagram shows that (^{226}Ra)/[Ba] for each plagioclase separate is higher than expected for crystallization from the host liquid, even when the effects of differential partitioning of Ra and Ba are taken into account (Figure 8). Although Ra concentrations in minerals with initial ^{226}Ra-^{230}Th disequilibrium will change over time, the anomalously high (^{226}Ra)/[Ba] in the measured mineral separates cannot be explained simply by decay because plagioclase has (^{226}Ra)/(^{230}Th) > 1 and would therefore have had even higher (^{226}Ra)/[Ba] in the past (Figure 8). Furthermore, the high (^{226}Ra)/[Ba] cannot be explained by anomalously low Ba concentrations. Instead, based on

calculated and experimentally-derived partition coefficients (Blundy and Wood 2003a; Fabbrizio, et al. 2009), Ba concentrations are equal to or higher than predicted for a given An content at 1000-1200°C (see Figure 4 and supplementary Table 5), and Ra concentrations are much higher than expected (e.g., Ra concentrations are a factor of ~2-10 higher than expected for equilibrium crystallization, assuming An_{60-80} plagioclase at temperatures of 1000-1200°C and using published partition coefficients (Blundy and Wood 2003a; Fabbrizio, et al. 2009)).

5.2 Nature of the source of plagioclase crystals

The implication of the preceding observations is that the macroscopic crystals present in each of these Krafla samples did not crystallize from their host liquids and instead represent crystals entrained during transport of the magma to the surface. Textural observations of dissolution surfaces cross-cutting crystal margins in clusters supports this interpretation (Fig. 2). The origin of the macroscopic crystals is difficult to define in detail. However, the isotopic and trace-element evidence can provide some additional insights into the nature of the source of the plagioclase in these samples. First, the chemical and isotopic heterogeneity within the plagioclase populations (and between plagioclase populations) that is evident in all of the different types of analyses presented here indicates that the crystals were derived from a chemically heterogeneous source region, and that the composition of that heterogeneous source changed from north to south along the eruptive fissure. Second, the low $\delta^{18}O$ of plagioclase compared to equilibrium with the host liquid suggests that the source of plagioclase either had experienced hydrothermal alteration after plagioclase crystallization, or had assimilated hydrothermally-altered material into the source melt prior to plagioclase crystallization. Third, the relatively high trace-element concentrations in plagioclase (e.g., Ba) compared to equilibrium with the host liquid suggests that the liquid from which the plagioclase crystallized was more chemically evolved than the host liquid. And finally, the observation of significant ^{226}Ra-^{230}Th disequilibria in all of the analyzed plagioclase separates suggests that they crystallized recently (within the past ~10 kyr).

Considered collectively, these observations point to a heterogeneous crystal mush as the most likely source of the plagioclase crystals in the samples studied here. A model where the ascending host liquid entrained crystals from different regions of a heterogeneous crystal mush is consistent with the wide compositional diversity within plagioclase, and with the textural observations indicating that some crystals were incorporated as coherent clusters that

subsequently experienced resorption along the edges of the crystal clusters. This model is also consistent with previous observations of oxygen-isotope heterogeneity within crystals at Laki (Bindeman, et al. 2006), and numerous studies documenting the importance of mush in producing compositional variation in Icelandic lavas (Carley, et al. 2011; Gurenko and Sobolev 2006; Maclennan, et al. 2003; Neave, et al. 2013; Passmore, et al. 2012; Thomson and Maclennan 2013).

5.3 Time scale estimates

Our data thus support previous models where most of the macroscopic crystals in Icelandic lavas were incorporated into the host liquid from a crystal mush during transport through the crust (Gurenko and Sobolev 2006; Hansen and Gronvold 2000; Neave, et al. 2014; Passmore, et al. 2012; Thomson and Maclennan 2013). A novel aspect of this study, however, is that we can use the combination of U-series data and the time scales of diffusive equilibration of oxygen-isotope and trace-element compositions to constrain the time scales of crystallization of plagioclase, storage of crystals within the crystal mush, and storage/ascent of the magma after incorporation of crystals into the host liquids. A conceptually similar approach was taken by Bindeman et al. (2006), who interpreted oxygen-isotope mineral data together with whole-rock U-series disequilibria in terms of the time scales of magma storage during crystallization and assimilation in a shallow reservoir. Our mush model of the origin of the plagioclase crystals is somewhat different (although Bindeman et al. (2006) did interpret some crystals with extreme $\delta^{18}O$ as derived from cumulates within the reservoir). Furthermore, we can provide additional constraints on time scales beyond that offered by Bindeman et al. (2006) by considering U-series disequilibria measured within the plagioclase crystals themselves, which allows us to also (albeit broadly) constrain the duration of storage of the crystals within the mush.

U-series crystallization ages for plagioclase are difficult to quantify precisely because the host liquid cannot be presumed to represent the exact composition of the melt(s) from which the plagioclase crystallized. However, some constraints can be obtained from the U-series data by comparison of the measured U-series data for plagioclase to those in Icelandic lavas, broadly considered. $(^{230}Th)/(^{232}Th)$ in most Icelandic lavas previously measured range from ~0.96 to 1.19, with higher activity ratios associated with basaltic compositions and lower activity ratios associated with dacites and rhyolites (Condomines, et al. 1981; Hemond, et al. 1988a; Kokfelt, et al. 2003; Kokfelt, et al. 2009; Koornneef, et al. 2012a; Sigmarsson 1996; Sigmarsson, et al.

1992a; Sigmarsson, et al. 1992b; Sigmarsson, et al. 1991; Zellmer, et al. 2008). Higher (^{230}Th)/(^{232}Th) and higher (^{230}Th)/(^{238}U) are also associated with larger distances to the plume center (Kokfelt, et al. 2003). Krafla lavas measured previously have activity ratios similar to those reported here. Therefore, the plagioclase-whole rock ^{238}U-^{230}Th isochron ages of 3.0 +6.1/-6.0 and 2.0 +9.1/-8.5 kyr for the samples studied here, which assume crystallization of plagioclase from liquids with (^{230}Th)/(^{232}Th) equal to that of the host lavas, are likely to be close to the true crystallization age. If the liquid from which the plagioclase crystallized had lower (^{230}Th)/(^{232}Th) than the host melt, the true ages would be younger than the ages calculated above. However, the calculated ages above are already within error of zero age, and therefore 1) the minimum age of crystallization of the plagioclase is within error of eruption, and 2) the liquid from which the plagioclase crystallized could not have had (^{230}Th)/(^{232}Th) significantly lower than the host liquid (which has measured (^{230}Th)/(^{232}Th) ~ 1.1). If, on the other hand, we assume a liquid (^{230}Th)/(^{232}Th) of 1.13 (near the maximum of that measured in main-rift Icelandic basalts previously), plagioclase crystallization ages would be 8.0 kyr and 8.8 kyr for 03KRA03 and 03KRA01, respectively.

These ^{238}U-^{230}Th crystallization ages are qualitatively consistent with the observation of ^{230}Th-^{226}Ra disequilibria in all plagioclase separates measured here. Because the measured (^{226}Ra)/[Ba] ratios are higher than equilibrium with the host liquids (Figure 8), ^{226}Ra-^{230}Th crystallization ages calculated assuming crystallization from the host are undefined. It is not possible to define a robust maximum age using a range of initial melt (^{226}Ra)/[Ba] in a manner analogous to the maximum ^{238}U-^{230}Th age discussed above because there are few ^{226}Ra measurements for Icelandic basalts and therefore the range for melts is poorly defined. However, because ^{226}Ra-^{230}Th disequilibria will decay to secular equilibrium within ~8-10 kyr (depending on the magnitude of the initial disequilibrium), at least some part of the crystals in the measured bulk separates must have crystallized recently. Thus, the U-series results taken together indicate a maximum (average) age of ~8-9 kyr for the plagioclase crystals scavenged from the mush and therefore a relatively short time frame for generation and storage of the crystal mush beneath Krafla. The U-Th age uncertainties are also consistent with much younger ages (within error of eruption age), which would imply even shorter time scales of storage of crystal mush. In fact, because (^{226}Ra)/(^{230}Th) measured in plagioclase is significantly higher than zero-age

crystallization from the host liquid, it is likely that crystallization ages were much younger (and likely substantially less than a half-life of ^{226}Ra).

The time frame between entrainment of the plagioclase in the host magma and eruption can also be constrained from our data. Diffusion at magmatic temperatures will act to equilibrate oxygen-isotope compositions and trace-element concentrations between zones within crystals. Using experimentally-determined diffusion rates, we can constrain the amount of time that any mush-derived crystals could have spent in the host liquid prior to eruption while still preserving the observed chemical and isotopic disequilibrium within the mineral separates and between the mineral separates and the host liquid. These maximum diffusion times therefore constrain the duration of storage of the erupted magma beneath the surface after interaction with the mush. We model diffusion of oxygen isotopes in plagioclase using a range of temperatures and grain sizes and the diffusion data of Elphick et al. (1988) for anorthite (Figure 9). We modeled the center retention time, which is the time at which the center of a crystal of a given radius begins to change composition (given by the time at which the dimensionless parameter Dt/a^2 is less than 0.03 where D is the diffusion coefficient, t is time, and a is the grain radius, assuming spherical geometry, following, for example, Cherniak and Watson (2010)). We also modeled the time to achieve 99% equilibration of the center of a spherical grain with the surroundings, using analytical solutions to the diffusion equation (equations 6.18 and 6.19 in Crank (1975)). These results therefore bracket the time of initial and final equilibration of the center of a grain of a given radius with its surrounding liquid.

The crystal populations studied here generally have widths (the limiting dimension for diffusion) of ~125-500 microns (Fig. 7). Therefore, all but the largest crystals would be effectively modeled with grain radii of ~60-250 microns. Given this range of radii, center retention times would be decades to a few centuries at temperatures of 1000°C, and times for 99% equilibration at the center would be decades to a few thousand years (Figure 9). The oxygen-isotope heterogeneity observed in replicate analyses of plagioclase from all size fractions of both of the analyzed samples suggests that the crystals preserve heterogeneity on the scale of 100 microns or smaller, and therefore suggest that these time scale estimates are upper limits. Furthermore, residence in a host liquid at higher temperatures would lead to faster diffusion (e.g., at 1200°C, heterogeneity would be preserved for only years to a few decades) again suggesting that these storage time estimates are maxima.

Diffusion of oxygen can also be used to constrain the time scales of storage of crystals in the mush prior to incorporation into the host liquid. In this case, we assume temperatures of ~700-800°C (corresponding to a range of possible mush temperatures). At these conditions, center retention times for oxygen in 100 micron diameter grains are thousands to tens of thousands of years, and 99% equilibration times are tens of thousands to millions of years (Figure 9). Therefore, these grains could easily have retained a signature of initial oxygen-isotope heterogeneity (or any heterogeneity introduced during storage as a mush) over the length of time that the plagioclase crystals existed (<~9 kyr). These results are also consistent with the preservation of Ba heterogeneity within the crystals, as Ba diffusion rates are orders of magnitude slower than oxygen in feldspar (e.g., Cherniak 2010).

In summary, the U-series data require that the plagioclase crystals studied here formed a maximum of ~8-9 kyr before the present (on average), and at least some parts of the crystal populations likely crystallized much more recently. Of that total time, the preservation of oxygen-isotope heterogeneity within and between crystals requires that the crystals spent a relatively short time in contact with their host liquids at high temperature; decades to centuries at storage temperatures of ~1000 °C, and years to decades with storage temperatures above 1200-1250°C. However, the oxygen-isotope heterogeneity observed could easily have been preserved for time scales exceeding the maximum crystallization ages at temperatures expected in a crystal mush (<700-800°C).

5.4 Implications for magmatic processes

Our results indicate that the macroscopic crystals in Krafla lavas originated as part of a young (likely less than a few thousand years old) crystal mush, and that they were entrained into the host liquids during magma ascent within decades to at most a few centuries prior to eruption. This in turn suggests a dynamic relationship between crystal mush within the crust and ascending magmas. Although mush zones could exist throughout the crustal column, the incorporation of chemically-distinct crystal populations into the two magmas which were erupted only a few kilometers apart, together with the consistent distinction in major element composition of magmas erupted at the north and south ends of the fissure system over the course of the eruption (Gronvold, et al. 2008) seems easiest to reconcile with storage of the analyzed crystals within a shallow crustal mush zone. The heterogeneity within crystals and between crystals within each sample also indicates that the mush zone from which the crystals were sourced is highly

compositionally heterogeneous. Oxygen-isotope heterogeneity *within* the crystal populations, in particular, suggests that magmas crystallizing plagioclase in localized areas of an upper crustal magma mush were subject to variable amounts of assimilation of hydrothermally-altered material prior to plagioclase crystallization, and that subsequent magmas passing through the system followed pathways that intersected chemically-diverse regions of the mush.

These conclusions are consistent with recent work showing that variable amounts of previously-existing crystalline material has been incorporated into the magma system at Laki (Bindeman, et al. 2012; Bindeman, et al. 2006; Gurenko and Sobolev 2006; Neave, et al. 2013; Passmore, et al. 2012; Thomson and Maclennan 2013), with evidence for variable amounts of incorporation of a middle- to lower-crustal mush into the Laki lavas (Neave, et al. 2013). Furthermore, the importance of mixing of multiple components of crystals within the lower Icelandic crust has also been documented (MacLennan 2008a; Maclennan 2008b). Maclennan (2008a) showed melt inclusion evidence for the incorporation of olivine crystals into Icelandic magmas during mixing and cooling of multiple magma batches. In addition, Maclennan (2008b) showed Pb isotopic variations in olivine-hosted melt inclusions, indicating that there was mixing of melts and crystals within the lower crust that were derived from an isotopically diverse source region.

Collectively, our work supports other recent studies in suggesting a model where erupted Icelandic magmas are the result of interaction of diverse magmas entering the crust, followed by complex interactions between melts and previously-crystallized material at all crustal levels. The mantle beneath Iceland has been shown to be heterogeneous on a short length scale (e.g., (Koornneef, et al. 2012b; Sims, et al. 2013a)) and the observed isotopic and chemical heterogeneity can be modeled as a function of the fusibility of these different mantle lithologies during glacially modulated melting (Sims, et al. 2013b). Furthermore, it appears that the heterogeneous melts contributing to the Icelandic crustal reservoir at multiple depths are recorded in some form in the crystal records in erupted lavas. Moreover, our data indicate that this recycling of material happens at multiple time scales, where crystallized material can be stored for short times (in our case, significantly less than ~9 kyr) prior to re-entrainment and that eruption follows entrainment by only decades to centuries, but that all of these time scales are rapid compared to the duration of volcanic activity in a given part of the Icelandic rift system.

Thus, it appears that Icelandic basalts, and basaltic lavas in general (cf. continental rift basalts: Sims et al., 2007; MORB: Zellmer et al., (2011) are likely to be generated by processes that are very similar to the processes of recharge and recycling of material that have been shown to be important in other tectonic settings and for more evolved lavas in arcs (e.g. Mount St. Helens, Cashman and Blundy (2013)) and continental rift settings (e.g. Mt Erebus (Sims et al., 2013a), but that the evidence for these processes is simply more subtle in basaltic systems than in arc and rift lavas where compositional distinctions may be greater. Furthermore, the time scales of crystallization, storage within a mush or near-solidus body, and recycling of crystal material are short relative to the duration of magmatic activity at a given volcanic center. These crystals thus provide an important window into sub-volcanic magmatic processes at both basaltic and intermediate systems.

6. Conclusions

1. Analysis of oxygen isotopes, major- and trace-element compositions, and U-series disequilibria in plagioclase crystals from samples of the Krafla Fires eruption at Krafla document the presence of multiple crystal populations within a single eruption, and even within a single hand sample.
2. The chemical and isotopic heterogeneity indicates that these crystals have distinct origins, and were derived from multiple sources. The trace-element concentrations and ^{230}Th-^{226}Ra disequilibria suggest that at least some of these crystals formed from evolved liquids and the oxygen-isotope variability indicates variable degrees of interaction of the source liquids with hydrothermally altered material. The most likely scenario is that the crystals were sourced from a heterogeneous mush zone.
3. Time scales of storage, evolution of melt within the presumed mush, and interaction with low-δ^{18}O material are all short, and in particular there can have been very little time between incorporation into host and eruption compared to the overall time of storage.
4. These observations, in conjunction with previous work, document a pattern whereby macroscopic crystals in basaltic magmas, like those in intermediate arc systems, originate within the crustal reservoir system and in general are not simply products of crystallization from the host liquid. They therefore represent an important archive of information about processes within the sub-volcanic storage system.

Acknowledgments

This project was supported by NSF awards EAR-0307691 and EAR-0714455 to KMC and EAR-0307123 to KWWS. Tracy Compton produced much of the barium data in feldspar as part of her senior thesis at UCD, and we thank Zhengrong Wang for running some of the oxygen-isotope analyses in the lab at Caltech.

Figure Captions:

Figure 1: Map showing sample locations. Main figure shows extent of lava flows erupted during the 1975-1984 Krafla Fires eruption (modified from (Sæmundsson 1991)), with sample locations marked (circles). Boundary of Krafla caldera (after Saemundsson et al., (2012) and Sims et al. (2013a)) is shown as bold dashed line. Inset shows location of Krafla central volcano within the Northern Rift Zone (dark shading; NRZ) of Iceland. The Eastern and Western Rift zones (ERZ and WRZ, respectively) are also shown.

Figure 2: SEM images and photomicrographs illustrating examples of the different plagioclase populations. (a): SEM image, showing cluster of large plagioclase crystals from Population 01-1. Panels (b) and (c) show photomicrographs (crossed polars) of parts of the same crystal cluster, with laser-ablation pits visible (dark circles). Note in (c) that resorption surface cross-cuts grain boundaries. (d): SEM image of elongate crystal from Population 01-2. (e): Cluster of two large, blocky, rounded grains from Population 03-1. Note that resorption surface cross-cuts grain boundaries. (f): SEM image of grain from Population 03-2 showing complex internal zoning (including resorbed core). Note that SEM images (panels a, d, e, and f) pre-date laser-ablation analyses, such that laser pits are not visible in these images. Note that brightness and contrast in some SEM images have been adjusted from the originals in order to better highlight zoning.

Figure 3: Chondrite-normalized rare-earth element plots for Krafla samples (chondrite values used for normalization from Nakamura, (1974)). (a): whole rock and groundmass analyses compared to compilation of previously-published analyses of Krafla lavas from the GeoRoc database (shaded field). Note that samples 03KRA02 and 03KRA01 have nearly-identical REE concentrations at this scale, as do samples 03KRA03 and 03KRA05. B) (b): Whole-rock and groundmass analyses from this study (shaded field) compared to REE analyses of plagioclase. Shown are data for dissolved bulk separates and averages of in-situ data by laser ablation ICP-MS. Note that for Population 03-2 laser data, Sm concentrations were below detection, so the value shown for Sm (the minimum value measured by laser-ablation in any of these samples) is an estimate of the maximum concentration. Data in the GeoRoc compilation for panel (a) are from the following references: (Arnorsson and Oskarsson 2007; Condomines, et al. 1983; Condomines, et al. 1981; David, et al. 2000; Fitton, et al. 2003; Grönvold and Mäkipää 1978; Hemond, et al. 1993; Kempton, et al. 2000; Kokfelt, et al. 2003; Kokfelt, et al. 2009; Koornneef, et al. 2012a; Koornneef, et al. 2012b; Kurz, et al. 1985; Maclennan, et al. 2001; Martin and Sigmarsson 2010; Nichols, et al. 2002; Nicholson, et al. 1991; Nicholson and Latin 1992; Sigvaldason and Oskarsson 1986; Slater, et al. 2001; Stracke, et al. 2003a; Stracke, et al. 2003b; Sveinbjornsdottir, et al. 1986; Tera, et al. 1986; Thirlwall, et al. 2004; Torssander 1988; White and Hochella 1992; Wood, et al. 1979)

Figure 4: Barium concentrations (in ppm) vs. anorthite concentrations (in mol % An) in plagioclase populations for Krafla samples 03KRA01 and 03KRA03. Concentrations of Ba were measured by laser-ablation ICP-MS. Anorthite content for the same spots was measured by electron microprobe for spots where Ba analyses were conducted at UCD and by laser-ablation ICP-MS where Ba analyses were conducted at OSU (see Methods for details). Also shown are curves for equilibrium Ba concentrations in plagioclase calculated as a function of An content. Different curves calculated using temperatures from 1000°C to 1200°C and partition coefficients predicted by Blundy and Wood (2003a) (BW) and measured experimentally by Fabbrizio et al.

(2009)(F) for 03KRA01 (grey lines, shown blue in the online version),and 03KRA03 (black lines), assuming that concentrations in the liquid were those of the whole-rock composition for each sample (i.e. 87.2 ppm for 03KRA01 and 63.1 ppm for 03KRA03). See legend for explanation of lines and symbols.

Figure 5: Oxygen-isotope compositions in plagioclase. Grey (blue in online version) and filled symbols show samples for 03KRA01 and 03KRA03, respectively. Small diamonds show data for individual aliquants of three different size fractions, and larger circles show mean and 1 standard deviation of all analyses for a single size fraction of a given sample. Typical 1-sigma reproducibility (1 standard deviation) of multiple analyses of a homogeneous sample is shown for comparison. Also shown are fields (grey/blue) for expected $\delta^{18}O$ of plagioclase in equilibrium with measured whole-rock compositions (squares). See text for explanation of calculation of equilibrium $\delta^{18}O_{plagioclase}$.

Figure 6: U-series isochron diagrams. (a) ^{238}U-^{230}Th isochron diagram showing data for plagioclase (plag), whole rock (wr) and groundmass (gm) analyses for each sample (03KRA01 – grey symbols (blue in online version); 03KRA03 – filled symbols). Large size fraction of plagioclase shown by larger symbols on diagram. Solid diagonal line indicates the equiline (secular equilibrium). Also shown are best-fit lines for data arrays for 03KRA01 (dashed line) and 03KRA03 (solid line). (b) ^{230}Th-^{226}Ra isochron diagram. Symbols as in panel (a).

Figure 7: Diagram showing comparison of crystal sizes for different types of analyses. Unfilled boxes indicate the three size fractions for oxygen-isotope analyses. Ruled boxes indicate small (horizontal ruling) and large (diagonal ruling) size fractions for U-series analyses. Thick bars show range of sizes of individual grain lengths (black) and widths (grey) for crystals analyzed for trace elements by laser-ablation ICP-MS; circles show mean sizes of analyzed crystals (mean not shown for Population 01-2 because of small sample size).

Figure 8: Ra evolution diagrams for (a) sample 03KRA01 and (b) sample 03KRA03. Curves show the evolution of (^{226}Ra)/[Ba] over time in whole-rock samples (wr) and in melt in equilibrium with plagioclase ($melt_{pl}$) over time. Composition of melt in equilibrium with plagioclase is calculated based on measured Ra, Ba and Th concentrations and Th isotopic compositions in plagioclase separates, together with predicted ((Blundy and Wood 2003a); BW) and measured ((Fabbrizio, et al. 2009); F) Ra and Ba partition coefficients for a range of temperatures and plagioclase compositions; see Cooper et al. (2001) for details of the method. Measured plagioclase compositions were first corrected for the presence of a small amount of glass in the bulk plagioclase separates (5% in small plagioclase fraction from 03KRA01 and the large size fraction from 03KRA03, and 7% in the small size fraction from 03KRA03), consistent with the maximum amount of glass possible based on mass-balance of U, Th, and Ba. Assuming less glass in the bulk separates has the effect of making (^{226}Ra)/[Ba] in the melt in equilibrium with plagioclase higher than what is shown. Curves for melt in equilibrium with plagioclase do not intersect the whole-rock curves (proxies for the erupted melt composition), indicating that the plagioclase separates were never in equilibrium with the host melt.

Figure 9: Summary of diffusion calculations. Figure shows center retention time (a) and time to 99% equilibration (b) for oxygen diffusion in plagioclase, as a function of grain radius, modeled

using the diffusion data of Elphick et al. (1988) for anorthite. Curves are shown for a range of temperatures from those relevant to storage of crystals in a mush to those relevant for entrainment of crystals in a mafic host melt. Grey shaded regions indicate the range of grain radii corresponding to the different crystal populations studied here. See text for further discussion.

References Cited:

Arnorsson S, Oskarsson N (2007) Molybdenum and tungsten in volcanic rocks and in surface and < 100 degrees C ground waters in Iceland. Geochimica Et Cosmochimica Acta 71(2):284-304 doi:10.1016/j.gca.2006.09.030

Ball L, Sims KWW, Schwieters J (2008) Measurement of 234U/238U and 230Th/232Th in volcanic rocks using the Neptune MC-ICP-MS. Journal of Analytical Atomic Spectroscopy 23:173-180

Bindeman I, Gurenko A, Carley T, Miller C, Martin E, Sigmarsson O (2012) Silicic magma petrogenesis in Iceland by remelting of hydrothermally altered crust based on oxygen isotope diversity and disequilibria between zircon and magma with implications for MORB. Terra Nova 24(3):227-232 doi:10.1111/j.1365-3121.2012.01058.x

Bindeman I, Sigmarsson O, Eiler JM (2006) Time constraints on the origin of large volume basalts derived from O-isotope and trace element mineral zoning and U-series disequilibria in the Laki and Grímsvötn volcanic system. Earth and Planetary Science Letters 245:245-259

Bindeman IN, Davis AM (2000) Trace element partitioning between plagioclase and melt: Investigation of dopant influence on partition behavior. Geochimica Et Cosmochimica Acta 64:2863-2878

Blundy J, Cashman K (2008) Petrologic Reconstruction of Magmatic System Variables and Processes. In: Putirka KD, Tepley FJ (eds) Minerals, Inclusions and Volcanic Processes, vol 69. pp 179-239

Blundy J, Wood B (2003a) Mineral-melt partitioning of uranium, thorium and their daughters. In: Bourdon B, Henderson GM, Lundstrom CC, Turner SP (eds) Uranium-Series Geochemistry, vol 52. pp 59-123

Blundy J, Wood B (2003b) Partitioning of trace elements between crystals and melts. Earth and Planetary Science Letters 210:383-397

Borthwick J, Harmon RS (1982) A note regarding ClF 3 as an alternative to BrF 5 for oxygen isotope analysis. Geochimica et Cosmochimica Acta 46:1665-1668

Burgisser A, Bergantz GW (2011) A rapid mechanism to remobilize and homogenize highly crystalline magma bodies. Nature 471(7337):212-215 doi:Doi 10.1038/Nature09799

Carley T, Miller C, Wooden J, Bindeman I, Barth A (2011) Zircon from historic eruptions in Iceland: reconstructing storage and evolution of silicic magmas. Mineralogy and Petrology 102(1-4):135-161 doi:10.1007/s00710-011-0169-3

Cashman K, Blundy J (2013) Petrological cannibalism: the chemical and textural consequences of incremental magma body growth. Contributions to mineralogy and petrology/Beitrage zur Minerologie und Petrologie Berlin and New York NY 166(3):703-729 doi:http://dx.doi.org/10.1007/s00410-013-0895-0

Cheng H, Edwards RL, Shen C-C, Polyak VJ, Asmerom Y, Woodhead J, Hellstrom J, Wang Y, Kong X, Spotl C, Wang X, Alexander Jr. EC (2013) Improvements in 230Th dating, 230Th and 234U half-life values, and U-Th isotopic measurements by multi-collectro inductively coupled plasma mass spectrometry. Earth and Planetary Science Letters 371-372:82-91

Cherniak DJ (2010) Cation diffusion in feldspars. In: Zhang Y, Cherniak DJ (eds) Diffusion in Minerals and Melts: Reviews in Mineralogy and Geochemistry, v 72, vol., pp 691-733
Cherniak DJ, Watson EB (2010) Li diffusion in zircon. Contributions to Mineralogy and Petrology 160(3):383-390 doi:10.1007/s00410-009-0483-5
Chiba H, Chacko T, Clayton RN, Goldsmith JR (1989) Oxygen isotope fractionations involving diopside, forsterite, magnetite, and calcite: Application to geothermometry. Geochimica et Cosmochimica Acta 53:2985-2995
Clague DA (1987) Hawaiian xenolith populations, magma supply rates, and development of magma chambers. Bulletin of Volcanology 49:577-587
Clayton RN, Mayeda TK (1963) The use of bromine pentafluoride in the extraction of oxygen from oxides and silicates for isotopic analysis. Geochimica Et Cosmochimica Acta 27:43-52
Clynne MA (1999) A complex magma mixing origin for rocks erupted in 1915, Lassen Peak, California. Journal of Petrology 40(1):105-132
Condomines M, Gronvold K, Hooker PJ, Muehlenbachs K, Onions RK, Oskarsson N, Oxburgh ER (1983) Helium, Oxygen, Strontium and Neodymium Isotopic Relationships in Icelandic Volcanics. Earth and Planetary Science Letters 66(1-3):125-136 doi:Doi 10.1016/0012-821x(83)90131-0
Condomines M, Morand P, Allegre CJ (1981) 230Th-238U disequilibria in historical lavas from Iceland. Earth and Planetary Science Letters 55:393-406
Cooper K, M., Kent AJR (2014) Rapid remobilisation of magmatic crystals kept in cold storage. Nature 506(7849):480-483 doi:10.1038/nature12991
Cooper KM (2009) Comment on "On the recent bimodal magmatic processes and their rates in the Torfajökull –Veidivötn area, Iceland" by G.F. Zellmer, K.H. Rubin, K. Grönvold, and Z. Jurado-Chichay. Earth and Planetary Science Letters 281:110-114
Cooper KM, Donnelly CT (2008) ^{238}U-^{230}Th-^{226}Ra Disequilibria in dacite and plagioclase from the 2004-2005 eruption of Mount St. Helens. In: Sherrod DR, Scott WE, Stauffer PH (eds) A Volcano Rekindled: The Renewed Eruption at Mount St Helens, 2004-2006, vol. US Geological Survey Professional Paper 1750, pp 827-846
Cooper KM, Eiler JM, Asimow PD, Langmuir CH (2004) Oxygen-isotope evidence for the origin of enriched mantle beneath the mid-Atlantic ridge. Earth and Planetary Science Letters 220(3-4):297-316
Cooper KM, Reid MR (2008) Uranium-series Crystal Ages. In: Putirka K, Tepley III FJ (eds) Minerals, Inclusions and Volcanic Processes: Reviews in Mineralogy and Geochemistry, vol 69. pp 479-544
Cooper KM, Reid MR, Murrell MT, Clague DA (2001) Crystal and magma residence at Kilauea Volcano, Hawaii: ^{230}Th-^{226}Ra dating of the 1955 east rift eruption. Earth and Planetary Science Letters 184(3-4):703-718
Coplen TB (1996) New guidelines for the reporting of stable hydrogen, carbon, and oxygen isotope ratio data. Geochimica et Cosmochimica Acta 60(3359-3360)
Costa F, Andreastuti S, de Maisonneuve CB, Pallister JS (2013) Petrological insights into the storage conditions, and magmatic processes that yielded the centennial 2010 Merapi explosive eruption. Journal of Volcanology and Geothermal Research 261:209-235 doi:10.1016/j.jvolgeores.2012.12.025
Costa F, Coogan LA, Chakraborty S (2010) The time scales of magma mixing and mingling involving primitive melts and melt-mush interaction at mid-ocean ridges. Contributions to Mineralogy and Petrology 159(3):371-387 doi:10.1007/s00410-009-0432-3

Costa F, Dohmen R, Chakraborty S (2008) Time scales of magmatic processes from modeling the zoning patterns of crystals. In: Putirka K, Tepley III FJ (eds) Minerals, Inclusions and Volcanic Processes: Reviews in Mineralogy and Geochemistry: Reviews in Mineralogy and Geochemistry, vol 69. pp 545-594

Crank J (1975) The mathematics of diffusion. Oxford University Press, Oxford

David K, Schiano P, Allegre CJ (2000) Assessment of the Zr/Hf fractionation in oceanic basalts and continental materials during petrogenetic processes. Earth and Planetary Science Letters 178(3-4):285-301 doi:Doi 10.1016/S0012-821x(00)00088-1

Davidson JP, Hora JM, Garrison JM, Dungan MA (2005) Crustal forensics in arc magmas. Journal of Volcanology and Geothermal Research 140:157-170

Degruyter W, Huber C (2014) A model for eruption frequency of upper crustal silicic magma chambers. Earth and Planetary Science Letters 403:117-130

Druitt TH, Costa F, Deloule E, Dungan M, Scaillet B (2012) Decadal to monthly timescales of magma transfer and reservoir growth at a caldera volcano. Nature 482(7383):77-U97 doi:10.1038/nature10706

Eichelberger JC (1978) Andesitic volcanism and crustal evolution. Nature 275:21-26

Eiler JM (2001) Oxygen isotope variations of basaltic lavas and upper mantle rocks. Reviews in Mineralogy and Geochemistry 43:319-364

Eiler JM, Carr MJ, Reagan M, Stolper E (2005) Oxygen isotope constraints on the sources of Central American arc lavas. Geochemistry Geophysics Geosystems 6

Eiler JM, Schiano P, Kitchen N, Stolper EM (2000) Oxygen-isotope evidence for recycled crust in the sources of mid-ocean-ridge basalts. Nature 403(6769):530-534

Elphick SC, Graham CM, Dennis PF (1988) An ion microprobe study of anhydrous oxygen diffusion in anorthite - a comparision with hydrothermal data and some geological implications. Contributions to Mineralogy and Petrology 100:490-495

Fabbrizio A, Schmidt MW, Gunther D, Eikenberg J (2009) Experimental determination of Ra mineral/melt partitioning for feldspars and 226Ra-disequilibrium crystallization ages of plagioclase and alkali-feldspar. Earth and Planetary Science Letters 280:137-148

Feineman MD, DePaolo DJ (2003) Steady-state Ra-226/Th-230 disequilibrium in mantle minerals: Implications for melt transport rates in island arcs. Earth and Planetary Science Letters 215(3-4):339-355

Fitton JG, Saunders AD, Kempton PD, Hardarson BS (2003) Does depleted mantle form an intrinsic part of the Iceland plume? Geochemistry Geophysics Geosystems 4 doi:Artn 1032 10.1029/2002gc000424

Garrison JM, Reagan MK, Sims KWW (2012) Dacite formation at Ilopango Caldera, El Salvador: U-series disequilibrium and implications for petrogenetic processes and magma storage time. Geochemistry Geophysics Geosystems 13 doi:Q06018 10.1029/2012gc004107

Gronvold K, Halldorsson SA, Sigurdsson G, Sverrisdottir G, Oskarsson N (2008) Isotopic systematics of magma movement in the Krafla Central Volcano, North Iceland. Geochimica Et Cosmochimica Acta 72(12):A331-A331

Grönvold K, Mäkipää H (1978) Chemical composition of Krafla lavas 1975-1977. Nordic Volcanological Institute Report 78-16:1-49

Gurenko AA, Sobolev AV (2006) Crust-primitive magma interaction beneath neovolcanic rift zone of Iceland recorded in gabbro xenoliths from Midfell, SW Iceland. Contributions to Mineralogy and Petrology 151(5):495-520 doi:10.1007/s00410-006-0079-2

Hansen H, Gronvold K (2000) Plagioclase ultraphyric basalts in Iceland: the mush of the rift. Journal of Volcanology and Geothermal Research 98(1-4):1-32 doi:Doi 10.1016/S0377-0273(99)00189-4

Helz RT (1987) Diverse olivine types in lava of the 1959 eruption of Kilauea Volcano and their bearing on eruption dynamics. In: Decker RW, Wright TL, Stauffer PH (eds) Volcanism in Hawaii, US Geological Survey Professional Paper 1350, vol 1. pp 691-722

Hemond C, Arndt NT, Lichtenstein U, Hofmann AW, Oskarsson N, Steinthorsson S (1993) The Heterogeneous Iceland Plume - Nd-Sr-O Isotopes and Trace- Element Constraints. J Geophys Res-Solid Earth 98(B9):15833-15850

Hemond C, Condomines M, Fourcade S, Allegre CJ, Oskarsson N, Javoy M (1988a) Thorium, Strontium and Oxygen Isotopic Geochemistry in Recent Tholeiites from Iceland - Crustal Influence on Mantle-Derived Magmas. Earth and Planetary Science Letters 87(3):273-285 doi:Doi 10.1016/0012-821x(88)90015-5

Hemond C, Condomines M, Fourcade S, Allègre CJ, Oskarsson N, Javoy M (1988b) Thorium, strontium, and oxygen isotopic geochemistry in recent tholeiites from Iceland: crustal influence on mantle-derived magmas. Earth and Planetary Science Letters 87:273-285

Higgins MD, Roberge J (2007) Three magmatic components in the 1973 eruption of Eldfell volcano, Iceland: Evidence from plagioclase crystal size distribution (CSD) and geochemistry. Journal of Volcanology and Geothermal Research 161(3):247-260 doi:10.1016/j.jvolgeores.2006.12.002

Holden N (1990) Total half-lives for selected nuclides. Pure and Applied Chemistry 62:941-958

Jaffey AH, Flynn KF, Glendenin LE, Bentley WC, Essling AM (1971) Precision measurement of half-lives and specific activitites of 235U and 238U. Physical Review C 4:1889-1906

Kelley KA, Plank T, Ludden J, Staudigel H (2003) Composition of altered oceanic crust at ODP Sites 801 and 1149. Geochemistry Geophysics Geosystems 4 doi:Artn 8910 10.1029/2002gc000435

Kempton PD, Fitton JG, Saunders AD, Nowell GM, Taylor RN, Hardarson BS, Pearson G (2000) The Iceland plume in space and time: a Sr-Nd-Pb-Hf study of the North Atlantic rifted margin. Earth and Planetary Science Letters 177(3-4):255-271 doi:Doi 10.1016/S0012-821x(00)00047-9

Kent AJR, Blundy J, Cashman K, Cooper KM, Donnelly C, Pallister JS, Reagan M, Rowe MC, Thornber CR (2007) Vapor transport prior to the October 2004 eruption of Mount St. Helens, Washington: Insight from Li and 210Pb systematics. Geology

Kent AJR, Darr C, Koleszar AM, Salisbury MJ, Cooper KM (2010) Preferential eruption of andesitic magmas through recharge filtering. Nat Geosci 3(9):631-636 doi:Doi 10.1038/Ngeo924

Kilgour G, Blundy J, Cashman K, Mader HM (2013) Small volume andesite magmas and melt-mush interactions at Ruapehu, New Zealand: evidence from melt inclusions. Contributions to Mineralogy and Petrology 166(2):371-392 doi:10.1007/s00410-013-0880-7

Kokfelt TF, Hoernle K, Hauff F (2003) Upwelling and melting of the Iceland plume from radial variation of U-238-Th-230 disequilibria in postglacial volcanic rocks. Earth and Planetary Science Letters 214(1-2):167-186 doi:10.1016/S0012-821X(03)00306-6

Kokfelt TF, Hoernle K, Lundstrom C, Hauff F, van den Bogaard C (2009) Time-scales for magmatic differentiation at the Snaefellsjokull central volcano, western Iceland: Constraints from U-Th-Pa-Ra disequilibria in post-glacial lavas. Geochimica Et Cosmochimica Acta 73(4):1120-1144 doi:10.1016/j.gca.2008.11.021

Koornneef JM, Stracke A, Bourdon B, Gronvold K (2012a) The influence of source heterogeneity on the U-Th-Pa-Ra disequilibria in post-glacial tholeiites from Iceland. Geochimica Et Cosmochimica Acta 87:243-266 doi:10.1016/j.gca.2012.03.041
Koornneef JM, Stracke A, Bourdon B, Meier MA, Jochum KP, Stoll B, Gronvold K (2012b) Melting of a Two-component Source beneath Iceland. Journal of Petrology 53(1):127-157 doi:10.1093/petrology/egr059
Kurz MD, Meyer PS, Sigurdsson H (1985) Helium Isotopic Systematics within the Neovolcanic Zones of Iceland. Earth and Planetary Science Letters 74(4):291-305 doi:Doi 10.1016/S0012-821x(85)80001-7
Ludwig KR (2001) Isoplot 3.0 - A geochronological toolkit for Microsoft Excel. Berkeley Geochronology Center, Special Publication 4.
MacLennan J (2008a) Concurrent Mixing and Cooling of Melts under Iceland. Journal of Petrology 49(11):1931-1953 doi:10.1093/petrology/egn052
Maclennan J (2008b) Lead isotope variability in olivine-hosted melt inclusions from Iceland. Geochimica Et Cosmochimica Acta 72(16):4159-4176 doi:10.1016/j.gca.2008.05.034
Maclennan J, McKenzie D, Gronvold K, Shimizu N, Eiler JM, Kitchen N (2003) Melt mixing and crystallization under Theistareykir, northeast Iceland. Geochemistry Geophysics Geosystems 4 doi:Artn 8624
10.1029/2003gc000558
Maclennan J, McKenzie D, Gronvold K, Slater L (2001) Crustal accretion under northern Iceland. Earth and Planetary Science Letters 191(3-4):295-310 doi:Doi 10.1016/S0012-821x(01)00420-4
Marsh BD (1998) On the interpretation of crystal size distributions in magmatic systems. Journal of Petrology 39(4):553-599
Martin E, Sigmarsson O (2010) Thirteen million years of silicic magma production in Iceland: Links between petrogenesis and tectonic settings. Lithos 116(1-2):129-144 doi:10.1016/j.lithos.2010.01.005
Nakamura N (1974) Determination of REE, Ba, Fe, Mg, Na and K in carbonaceous and ordinary chondrites. Geochimica et Cosmochimica Acta 38:757-775
Neave DA, Maclennan J, Edmonds M, Thordarson T (2014) Melt mixing causes negative correlation of trace element enrichment and CO2 content prior to an Icelandic eruption. Earth and Planetary Science Letters 400:272-283 doi:10.1016/j.epsl.2014.05.050
Neave DA, Passmore E, Maclennan J, Fitton G, Thordarson T (2013) Crystal-Melt Relationships and the Record of Deep Mixing and Crystallization in the ad 1783 Laki Eruption, Iceland. Journal of Petrology 54(8):1661-1690 doi:10.1093/petrology/egt027
Nichols ARL, Carroll MR, Hoskuldsson A (2002) Is the Iceland hot spot also wet? Evidence from the water contents of undegassed submarine and subglacial pillow basalts. Earth and Planetary Science Letters 202(1):77-87 doi:Pii S0012-821x(02)00758-6
Doi 10.1016/S0012-821x(02)00758-6
Nicholson H, Condomines M, Fitton JG, Fallick AE, Gronvold K, Rogers G (1991) Geochemical and isotopic evidence for crustal assimilation beneath Krafla, Iceland. Journal of Petrology 32(5):1005-1020
Nicholson H, Latin D (1992) Olivine Tholeiites from Krafla, Iceland - Evidence for Variations in Melt Fraction within a Plume. Journal of Petrology 33(5):1105-1124

Passmore E, Maclennan J, Fitton G, Thordarson T (2012) Mush Disaggregation in Basaltic Magma Chambers: Evidence from the ad 1783 Laki Eruption. Journal of Petrology 53(12):2593-2623 doi:10.1093/petrology/egs061
Pyle DM, Ivanovich M, Sparks RSJ (1988) Magma-cumulate mixing identified by U-Th disequilibrium dating. Nature 331:187-189
Rubin KH, Zellmer GF (2009) Reply to Comment on "On the recent bimodal magmatic processes and their rates in the Torfajokull-Veidivotn area, Iceland" by KM Cooper Discussion. Earth and Planetary Science Letters 281(1-2):115-123 doi:DOI 10.1016/j.epsl.2009.02.008
Saal AE, Van Orman JA (2004) The Ra-226 enrichment in oceanic basalts: Evidence for melt-cumulate diffusive interaction processes within the oceanic lithosphere. Geochemistry Geophysics Geosystems 5:2003GC000620 doi:doi: 10.1029/2003GC000620
Sæmundsson K (1991) Jarðfræði Kröflukerfisins (Geology of the Krafla volcanic system). In: Gardarson A, Einarsson Á (eds) Náttúra Mývatns, vol. Hid íslenska náttúrufrædifélag, Reyjkavik, pp 25-95
Sæmundsson K, Hjartarson Á, Kaldal I, Sigurgeirsson MÁ, Kristinsson SG, Vikingsson S (2012) Geological map of the Northern volcanic zone, Icleand, Northern part. In, vol. Iceland GeoSurvey,
Schmitt AK (2011) Uranium Series Accessory Crystal Dating of Magmatic Processes. Annual Review of Earth and Planetary Sciences 39:321-349
Sharp ZD (1990) A laser-based microanalytical method for the in situ determination of oxygen isotope ratios of silicates and oxides. Geochimica et Cosmochimica Acta 54:1353-1357
Sigmarsson O (1996) Short magma chamber residence time at an Icelandic volcano inferred from U-series disequilibria. Nature 382(6590):440-442
Sigmarsson O, Condomines M, Fourcade S (1992a) A detailed Th, Sr and O isotope study of Hekla: differentiation processes in an Icelandic volcano. Contributions to Mineralogy and Petrology 112:20-34
Sigmarsson O, Condomines M, Fourcade S (1992b) Mantle and crustal contribution in the genesis of Recent basalts from off-rift zones in Iceland: Constraints from Th, Sr and O isotopes. Earth and Planetary Science Letters 110:149-162
Sigmarsson O, Hemond C, Condomines M, Fourcade S, Oskarsson N (1991) Origin of silicic magma in Iceland revealed by Th isotopes. Geology 19:621-624
Sigvaldason GE, Oskarsson N (1986) Fluorine in Basalts from Iceland. Contributions to Mineralogy and Petrology 94(3):263-271 doi:Doi 10.1007/Bf00371435
Sims KWW, Gill JB, Dosseto A, Hoffmann DL, Lundstrom Craig C, Williams RW, Ball L, Tollstrup D, Turner S, Prytulak J, Glessner JJG, Standish JJ, Elliott T (2008a) An inter-laboratory assessment of the thorium isotopic composition of synthetic and rock reference materials. Geostandards and Geoanalytical Research 32(1):65-91
Sims KWW, Hart SR, Reagan MK, Blusztain J, Staudigel H, Sohn RA, Layne GD, Ball LA, Andrews J (2008b) 238U-230Th-226Ra-210Pb-210Po, 232Th-228Ra and 235U-231Pa constraints on the ages and petrogenesis of Vailulu and Malumalu Lavas, Samoa. Geochemistry Geophysics Geosystems 9(Q04003):10.1029/2007GC001651
Sims KWW, Jr. RPA, Ramos FC, Sohn RA, Murrell MT, DePaolo DJ (2007) Determining eruption ages and erosion rates of Quaternary basaltic volcanism from combined U-series disequilibria and cosmogenic exposure ages. Geology 35:471-474

Sims KWW, Maclennan J, Blichert-Toft J, Mervine EM, Blusztajn J, Gronvold K (2013a) Short length scale mantle heterogeneity beneath Iceland probed by glacial modulation of melting. Earth and Planetary Science Letters 379:146-157 doi:10.1016/j.epsl.2013.07.027

Sims KWW, Pichat S, Reagan MK, Kyle PR, Dulaiova H, Dunbar NW, Prytulak J, Sawyer G, Layne GD, Blichert-Toft J, Gauthier PJ, Charette MA, Elliott TR (2013b) On the Time Scales of Magma Genesis, Melt Evolution, Crystal Growth Rates and Magma Degassing in the Erebus Volcano Magmatic System Using the U-238, U-235 and Th-232 Decay Series. Journal of Petrology 54(2):235-271 doi:Doi 10.1093/Petrology/Egs068

Slater L, McKenzie D, Gronvold K, Shimizu N (2001) Melt generation and movement beneath Theistareykir, NE Iceland. Journal of Petrology 42(2):321-354

Stelten ME, Cooper KM (2012) Constraints on the nature of the subvolcanic reservoir at South Sister volcano, Oregon from U-series dating combined with sub-crystal trace-element analysis of plagioclase and zircon. Earth and Planetary Science Letters 313:1-11 doi:Doi 10.1016/J.Epsl.2011.10.035

Stracke A, Zindler A, Salters VJM, McKenzie D, Blichert-Toft J, Albarede F, Gronvold K (2003a) Theistareykir revisited. Geochemistry Geophysics Geosystems 4 doi:Artn 8507
10.1029/2001gc000201

Stracke A, Zindler A, Salters VJM, McKenzie D, Gronvold K (2003b) The dynamics of melting beneath Theistareykir, northern Iceland. Geochemistry Geophysics Geosystems 4 doi:Artn 8513
10.1029/2002gc000347

Sveinbjornsdottir AE, Coleman ML, Yardley BWD (1986) Origin and History of Hydrothermal Fluids of the Reykjanes and Krafla Geothermal Fields, Iceland - a Stable Isotope Study. Contributions to Mineralogy and Petrology 94(1):99-109 doi:Doi 10.1007/Bf00371231

Tera F, Brown L, Morris J, Sacks IS, Klein J, Middleton R (1986) Sediment Incorporation in Island-Arc Magmas - Inferences from Be-10. Geochimica Et Cosmochimica Acta 50(4):535-550 doi:Doi 10.1016/0016-7037(86)90103-1

Thirlwall MF, Gee MAM, Taylor RN, Murton BJ (2004) Mantle components in Iceland and adjacent ridges investigated using double-spike Pb isotope ratios. Geochimica Et Cosmochimica Acta 68(2):361-386 doi:10.1016/S0016-7037(03)00424-1

Thomson A, Maclennan J (2013) The Distribution of Olivine Compositions in Icelandic Basalts and Picrites. Journal of Petrology 54(4):745-768 doi:Doi 10.1093/Petrology/Egs083

Thordarson T, Larsen G (2007) Volcanism in Iceland in historical time: Volcano types, eruption styles and eruptive history. J Geodyn 43(1):118-152 doi:10.1016/j.jog.2006.09.005

Torssander P (1988) Sulfur Isotope Ratios of Icelandic Lava Incrustations and Volcanic Gases. Journal of Volcanology and Geothermal Research 35(3):227-235 doi:Doi 10.1016/0377-0273(88)90019-4

Turner S, George R, Jerram DA, Carpenter N, Hawkesworth C (2003) Case studies of plagioclase growth and residence times in island arc lavas from Tonga and the Lesser Antilles, and a model to reconcile discordant age information. Earth and Planetary Science Letters 214(1-2):279-294

Valley JW, Kitchen N, Kohn MJ, Niendorff CR, Spicuzza MJ (1995) Strategies for high precision oxygen isotope analysis by laser fluorination. Geochimica et Cosmochimica Acta 59:5223-5231

Van Orman JA, Saal AE, Bourdon B, Hauri EH (2006) Diffusive fractionation of U-series radionuclides during mantle melting and shallow-level melt-cumulate interaction. Geochimica Et Cosmochimica Acta 70:4797-4812

White AF, Hochella MF (1992) Surface-Chemistry Associated with the Cooling and Subaerial Weathering of Recent Basalt Flows. Geochimica Et Cosmochimica Acta 56(10):3711-3721 doi:Doi 10.1016/0016-7037(92)90164-E

Wood DA, Joron JL, Treuil M, Norry M, Tarney J (1979) Elemental and Sr Isotope Variations in Basic Lavas from Iceland and the Surrounding Ocean-Floor - Nature of Mantle Source Inhomogeneities. Contributions to Mineralogy and Petrology 70(3):319-339 doi:Doi 10.1007/Bf00375360

Wright TL (1973) Magma mixing as illustrated by the 1959 eruption, Kilauea Volcano, Hawaii. Geological Society of America Bulletin 84:849-858

Zellmer G, Rubin K, Dulski P, Iizuka Y, Goldstein S, Perfit M (2011) Crystal growth during dike injection of MOR basaltic melts: evidence from preservation of local Sr disequilibria in plagioclase. Contributions to Mineralogy and Petrology 161(1):153-173 doi:10.1007/s00410-010-0518-y

Zellmer GF, Rubin KH, Gronvold K, Jurado-Chichay Z (2008) On the recent bimodal magmatic processes and their rates in the Torfajokull-Veidivotn area, Iceland. Earth and Planetary Science Letters 269:388-398

Figure 01

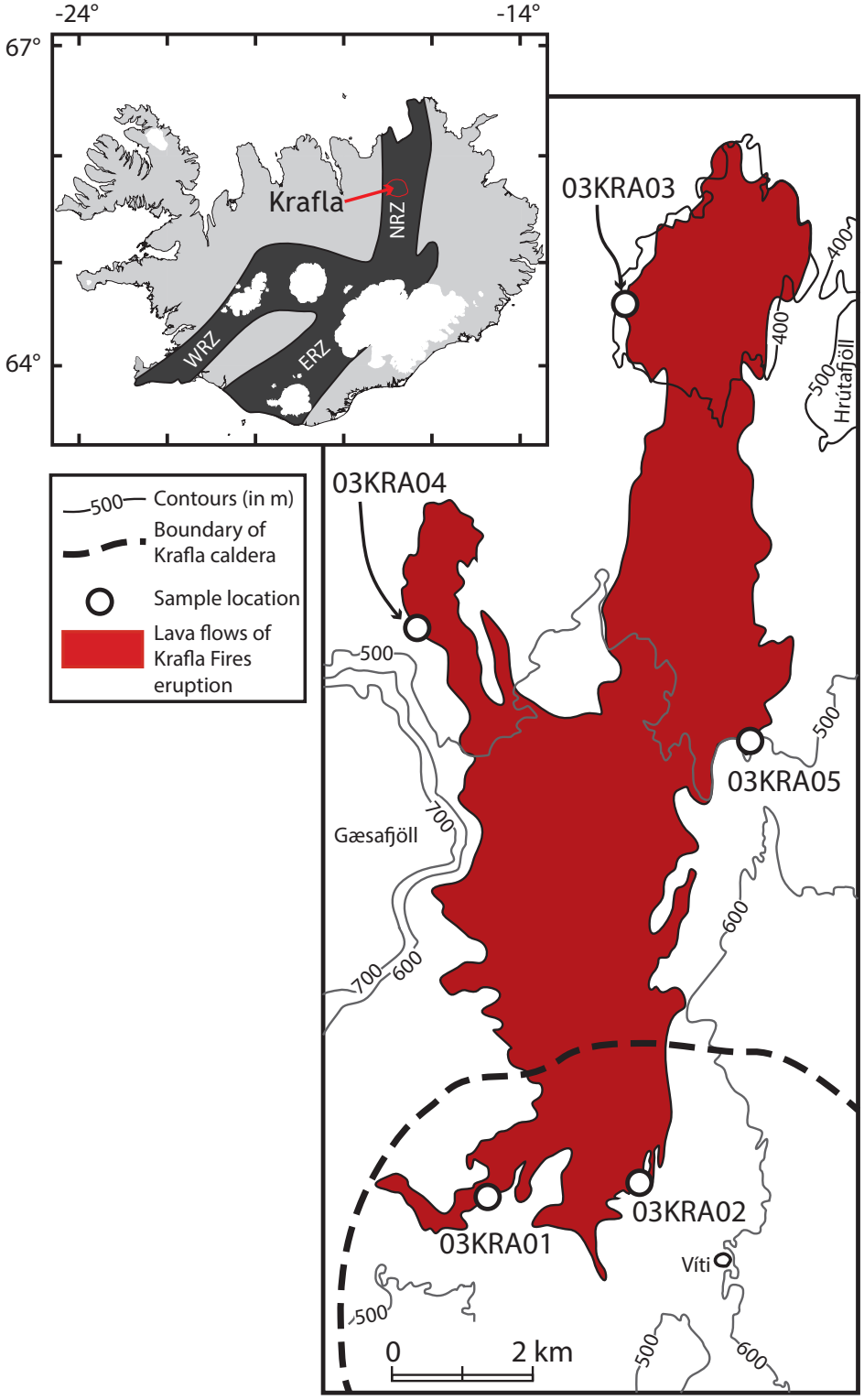

Cooper et al., Fig 1

Figure 02

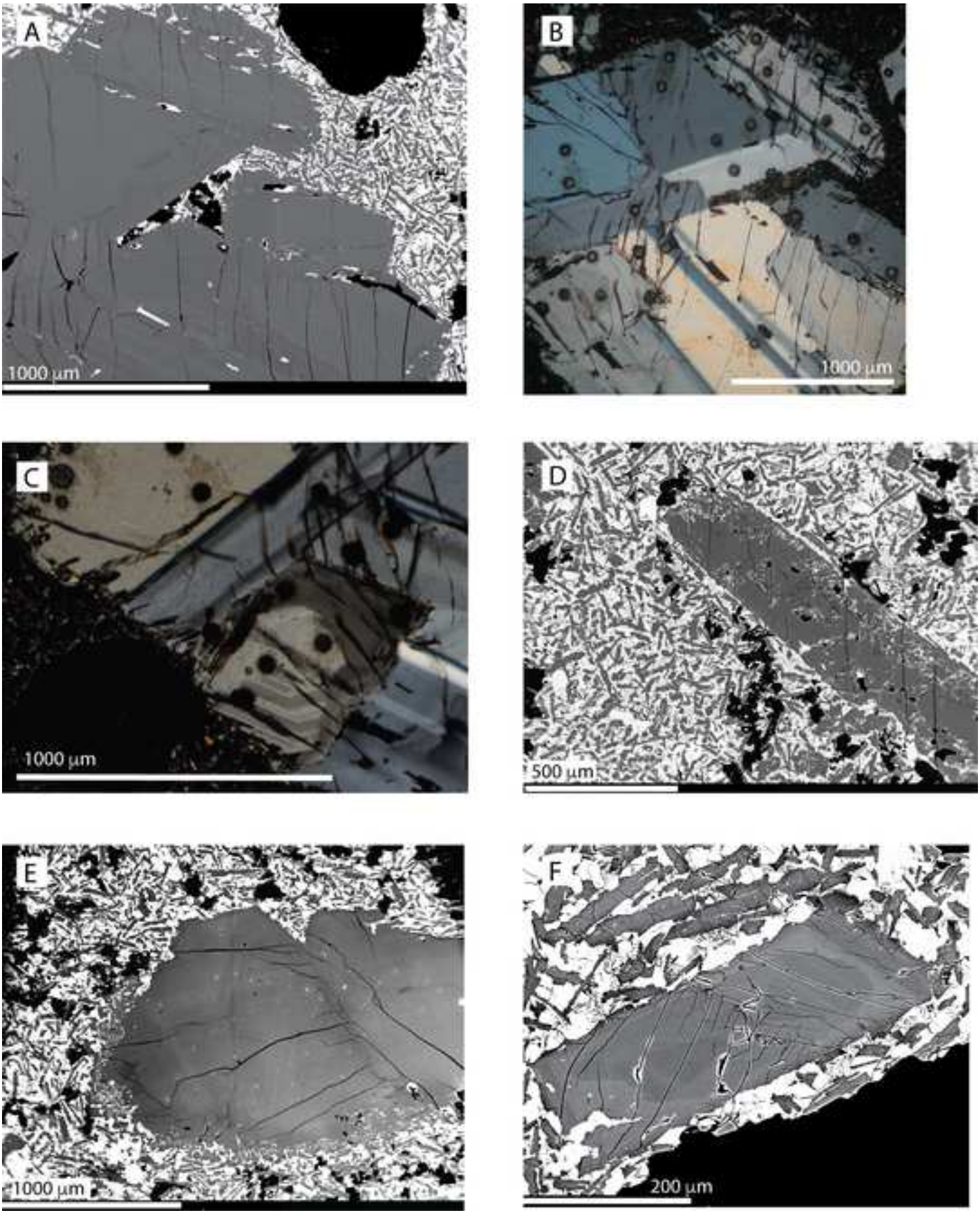

Figure 03

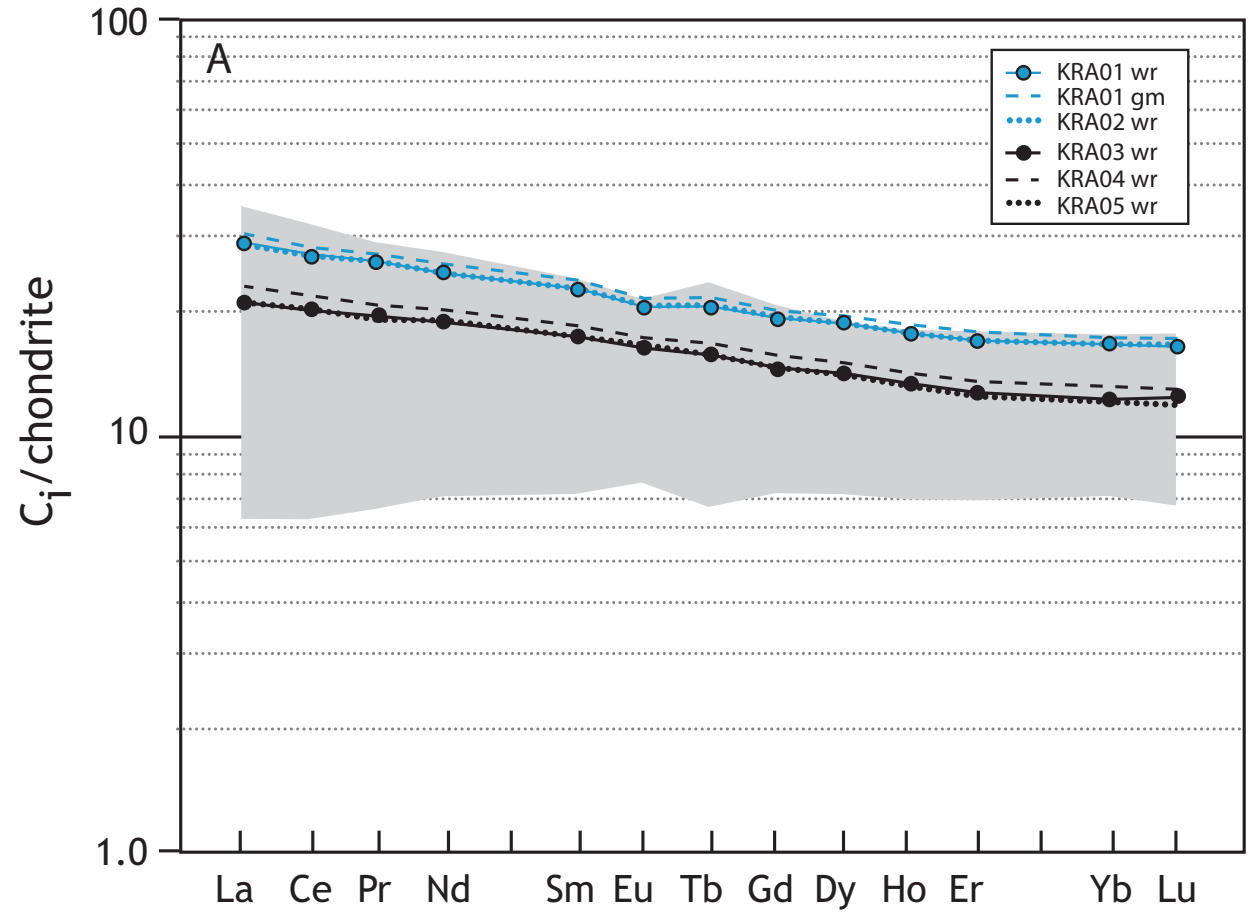

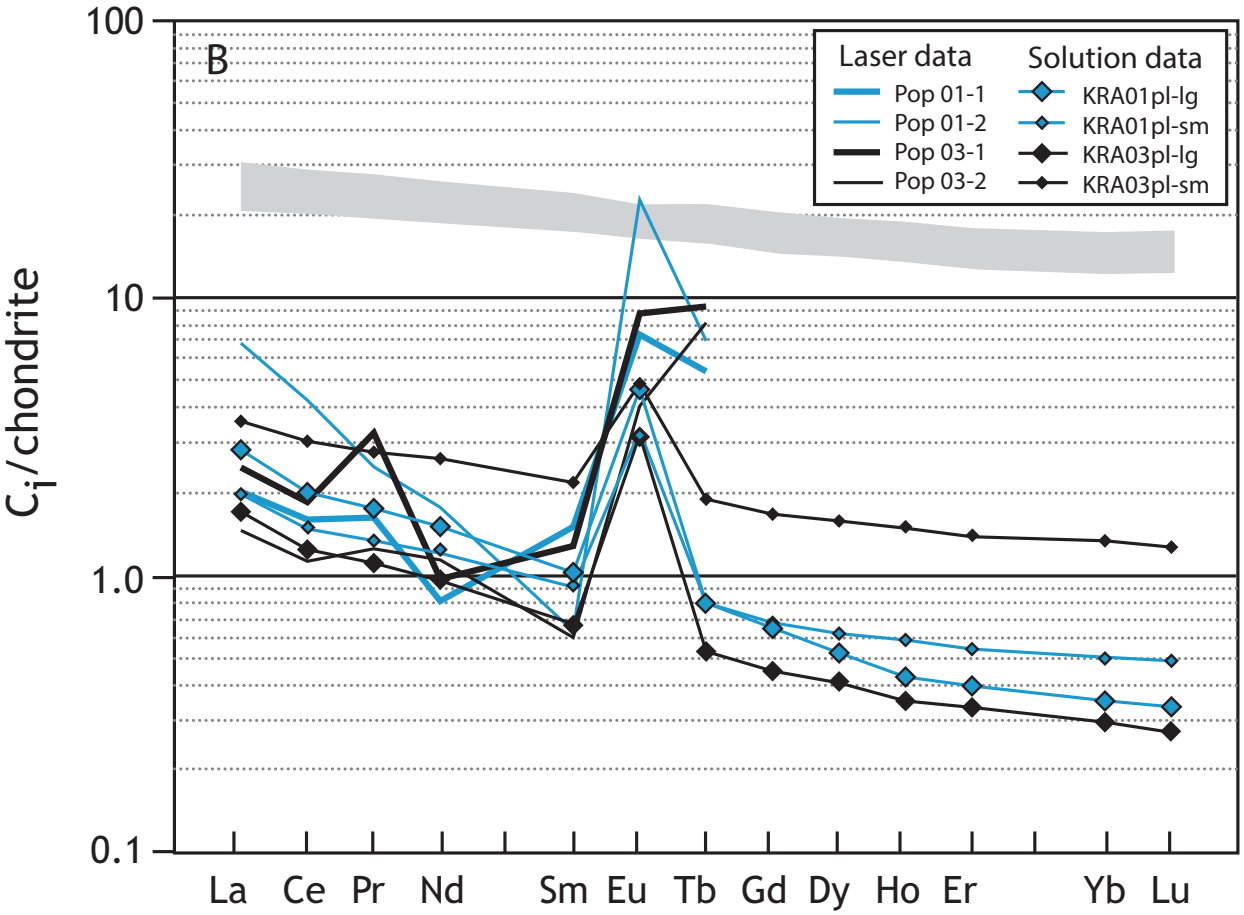

Cooper et al. Figure 3

Figure 04

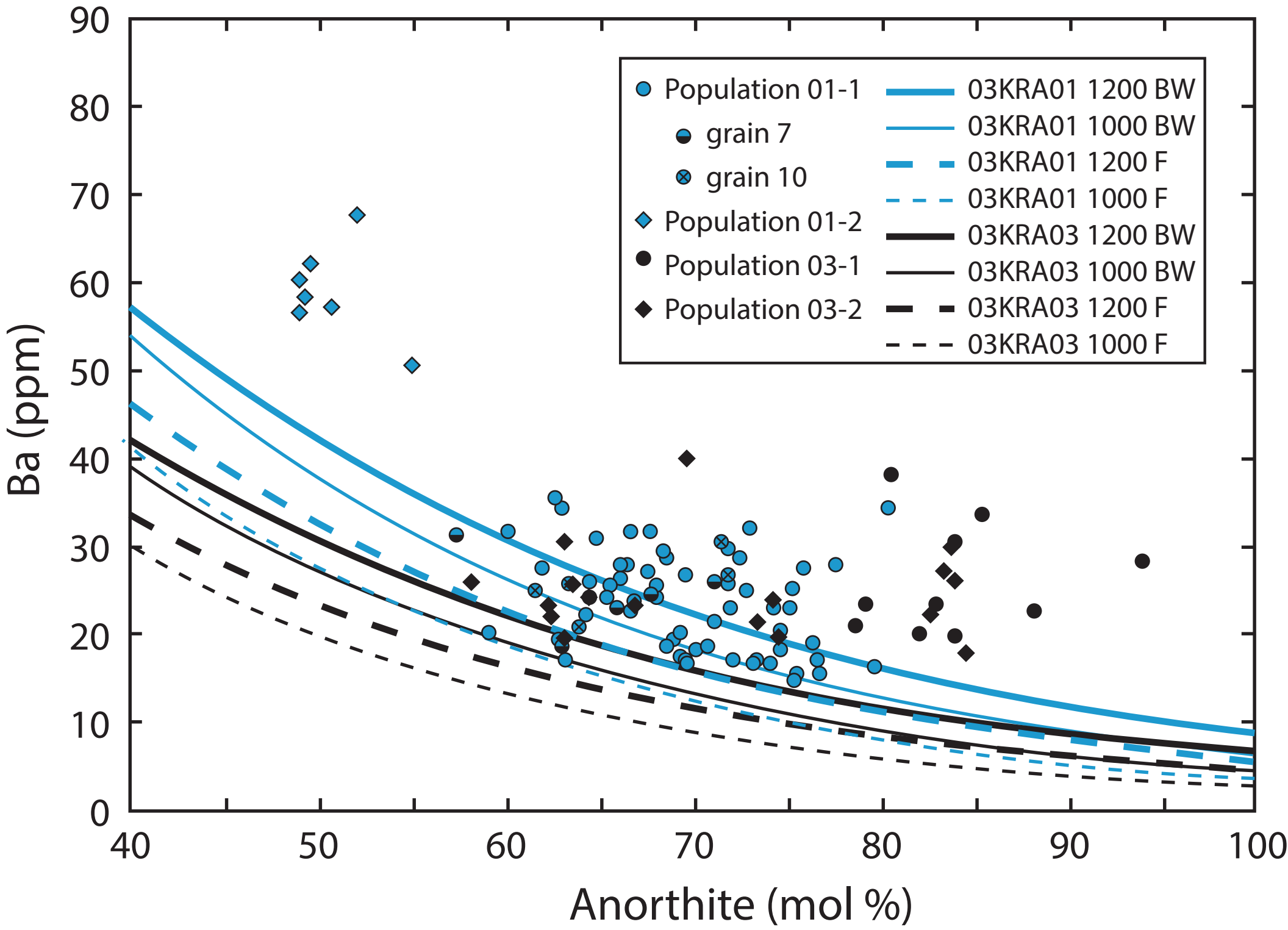
Ba (ppm)
Anorthite (mol %)
0
10
20
30
40
50
60
70
80
90
40
50
60
70
80
90
100
Population 01-1
grain 7
grain 10
Population 01-2
Population 03-1
Population 03-2
03KRA01 1200 BW
03KRA01 1000 BW
03KRA01 1200 F
03KRA01 1000 F
03KRA03 1200 BW
03KRA03 1000 BW
03KRA03 1200 F
03KRA03 1000 F

Figure 05

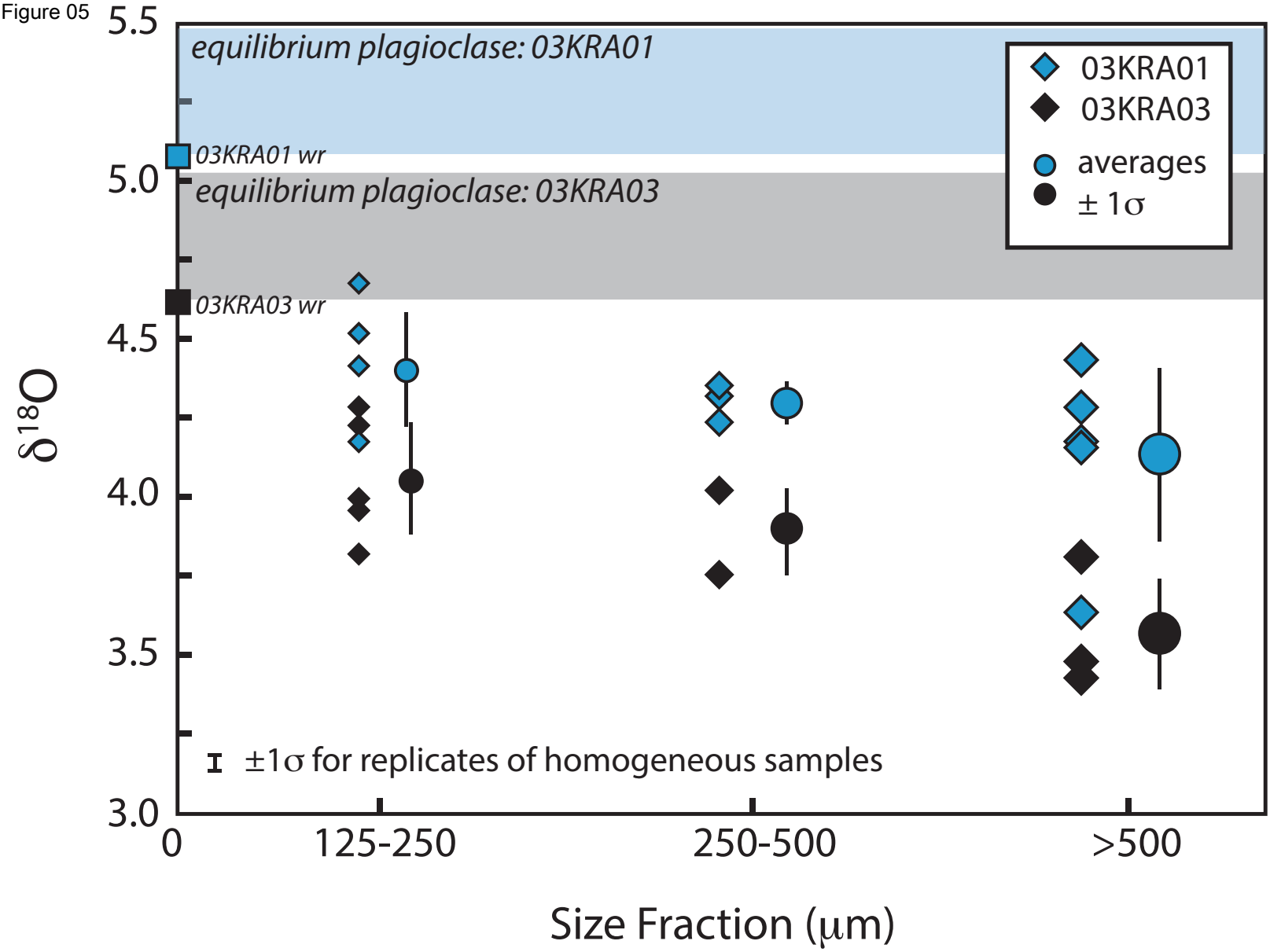

Cooper et al. Figure 5

Figure 06

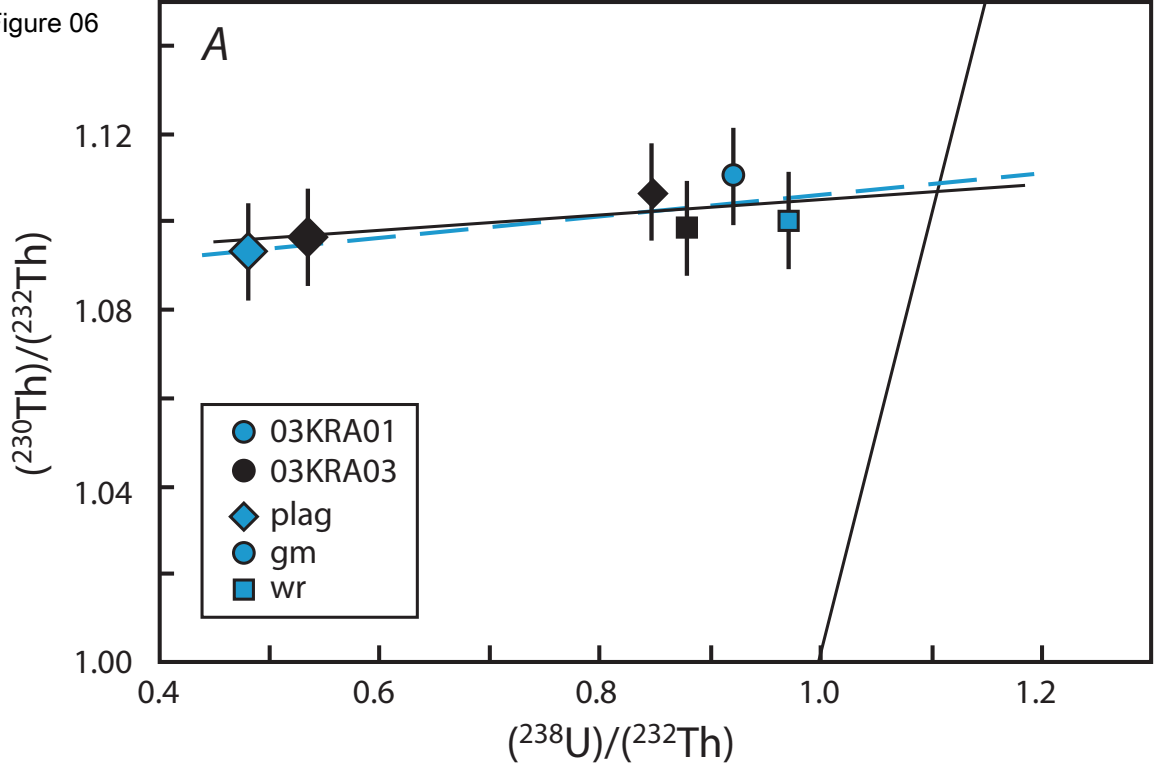
A
1.12
1.08
1.04
1.00
0.4
0.6
0.8
1.0
1.2
(230Th)/(232Th)
(238U)/(232Th)
03KRA01
03KRA03
plag
gm
wr

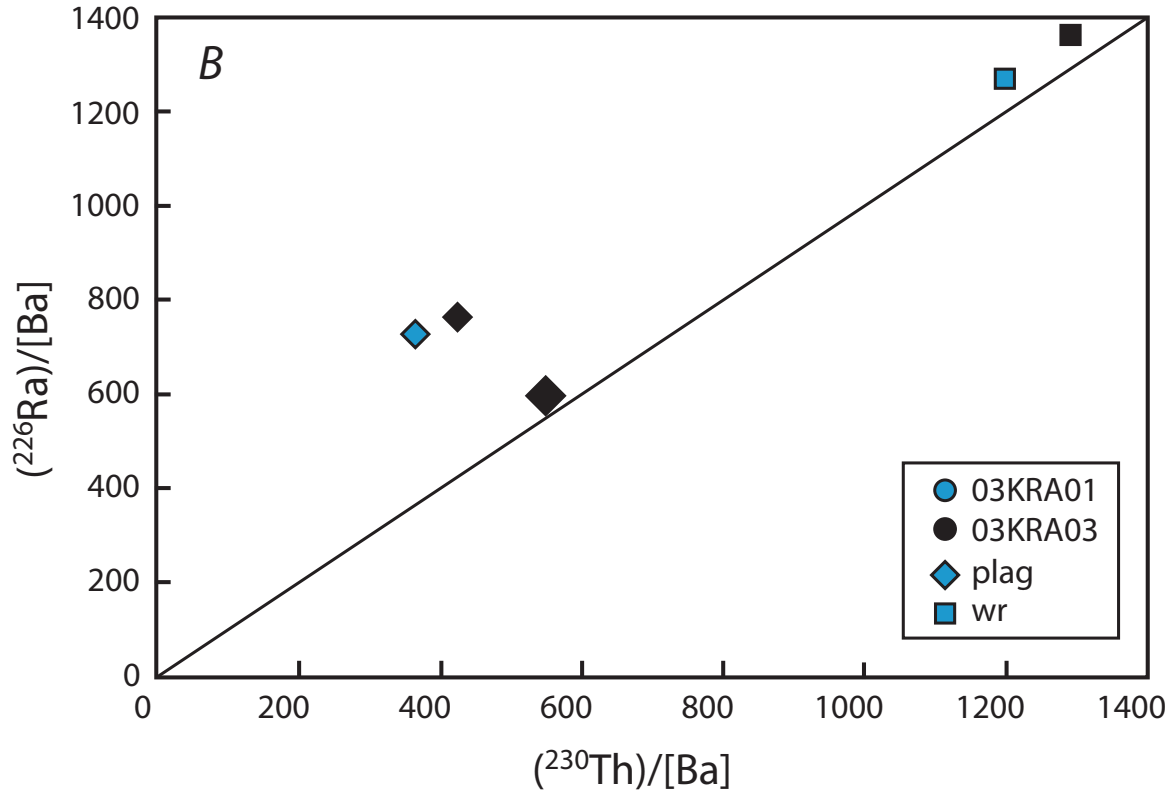
B
1400
1200
1000
800
600
400
200
0
0
200
400
600
800
1000
1200
1400
(226Ra)/[Ba]
(230Th)/[Ba]
03KRA01
03KRA03
plag
wr

Figure 07

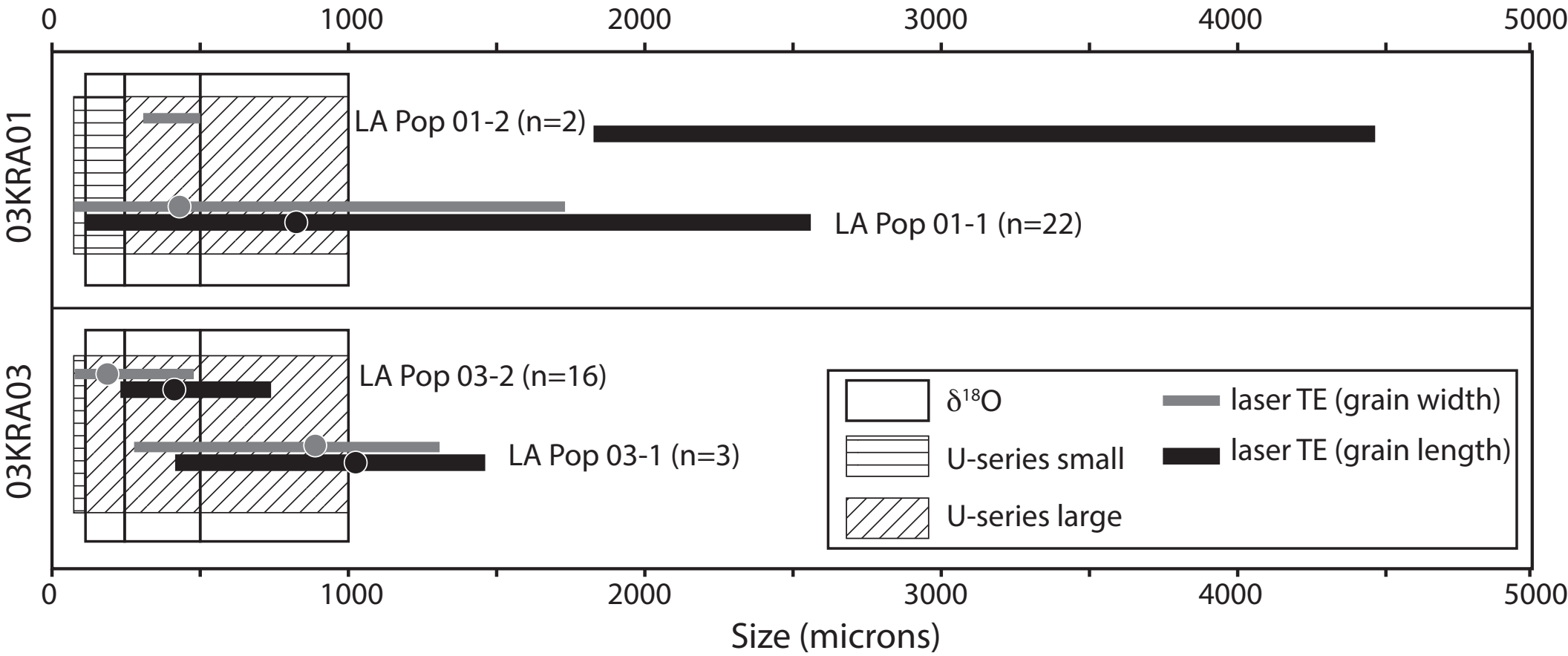

Cooper et al. Figure 7

Figure 08

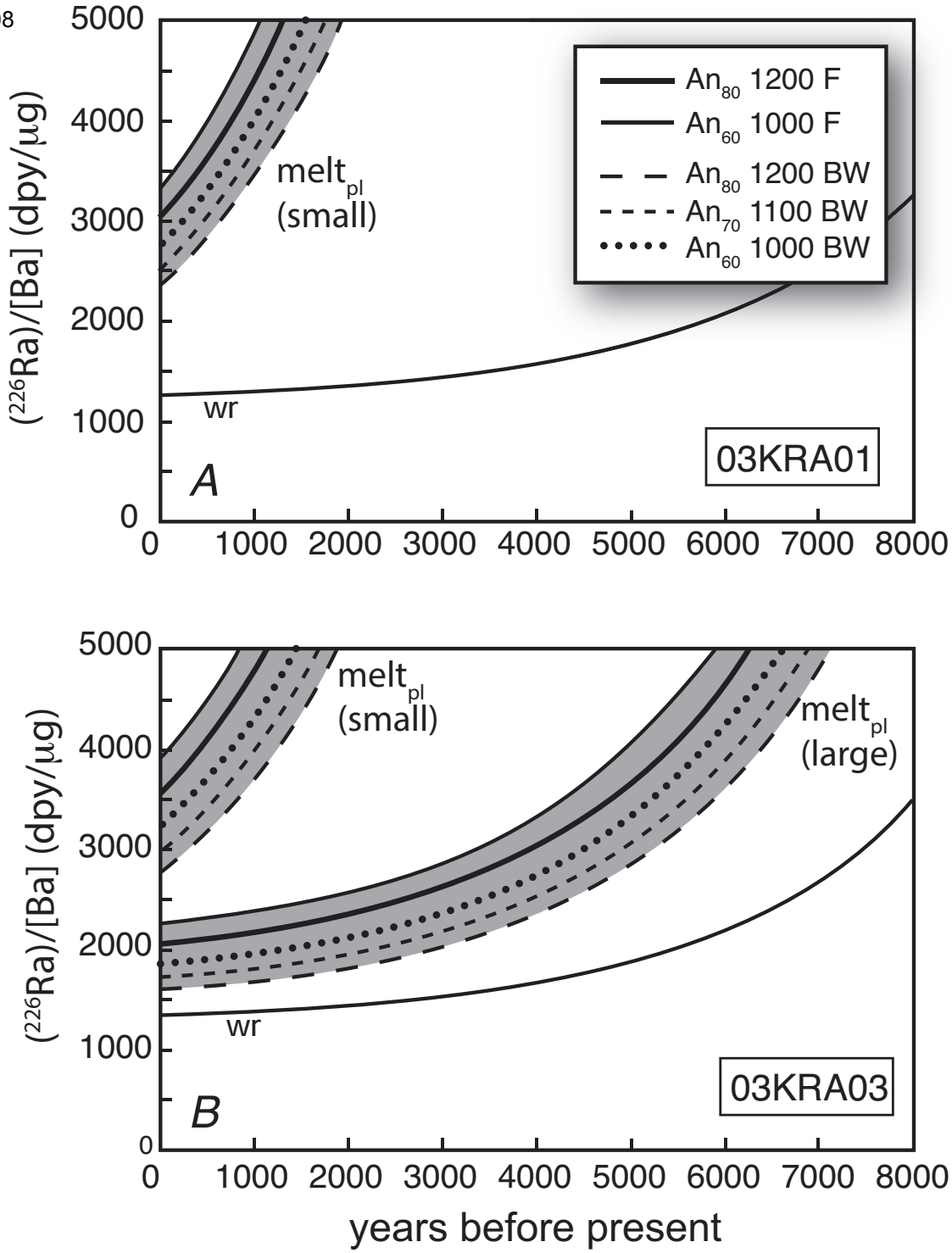

Cooper et al. Figure 8

Figure 09

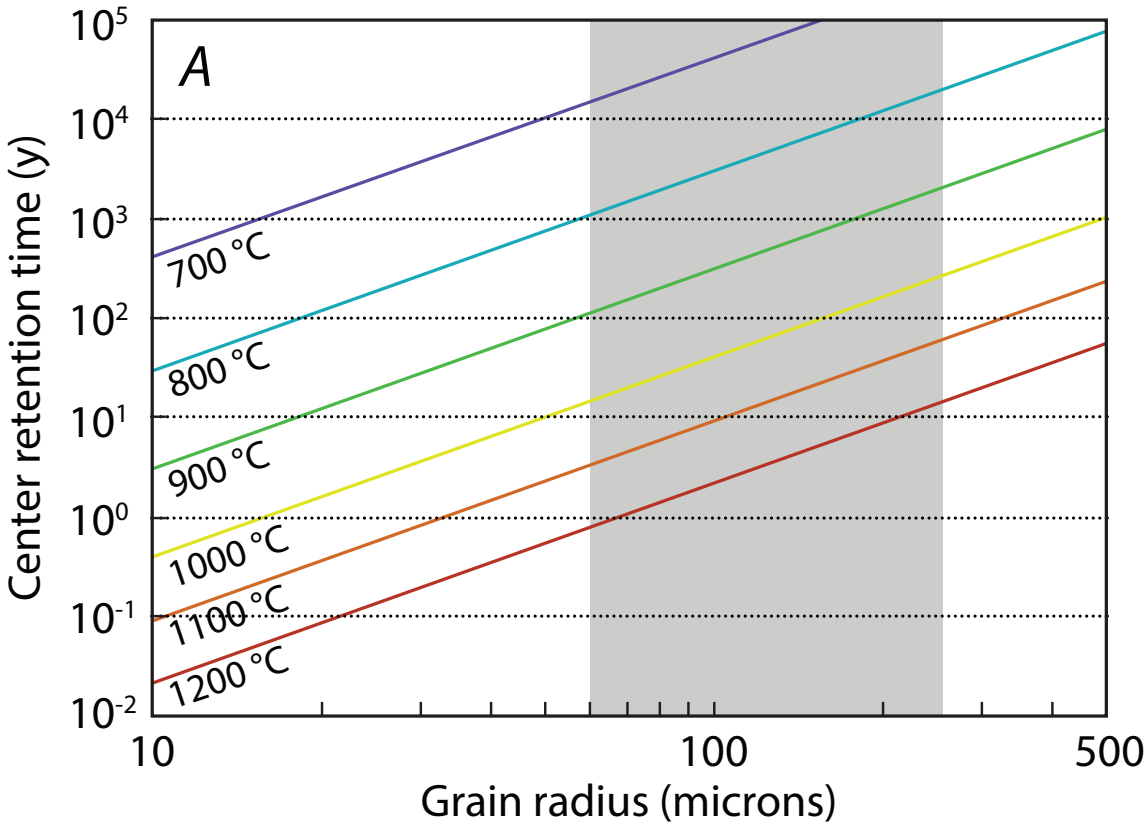

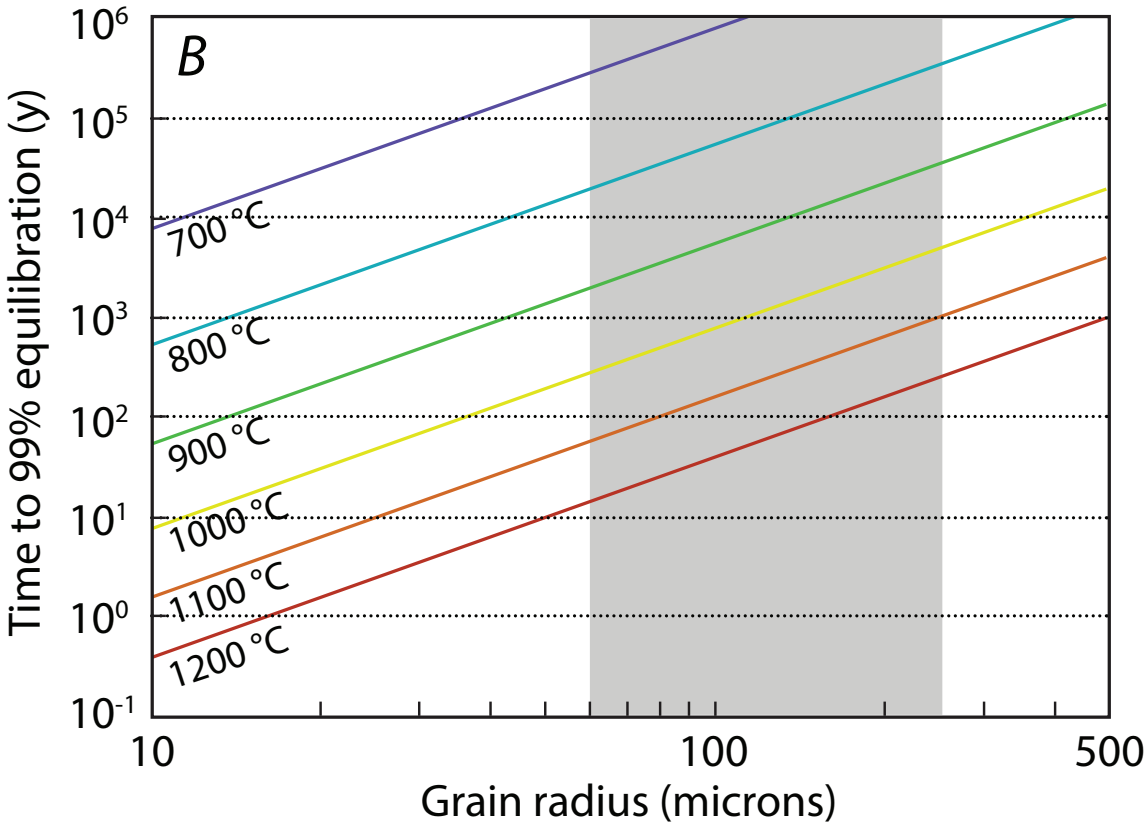

Cooper et al. Figure 9

Table 1: Oxygen-isotope measurements of plagioclase separates.

Sample name	$d^{18}O$ (‰)	(+/-), 1s[1]
03KRA01-500+	4.16	
03KRA01-500+	4.28	
03KRA01-500+	4.43	
03KRA01 500+	3.63	
03KRA01 500+	4.17	
03KRA01 500+ Average	*4.13*	*0.27*
03KRA01 250-500 mm	4.35	
03KRA01 250-500 mm	4.32	
03KRA01 250-500 mm	4.24	
03KRA01 250-500 mm Averag	*4.30*	*0.05*
03KRA01-125-250 mm	4.52	
03KRA01-125-250 mm	4.40	
03KRA01-125-250 mm	4.68	
03KRA01-125-250 mm	4.17	
03KRA01-125-250 mm	4.21	
03KRA01-125-250 mm Averag	*4.40*	*0.19*
03KRA03 500+	3.46	
03KRA03 500+	3.81	
03KRA03 500+	3.42	
03KRA03 500+ Average	*3.57*	*0.17*
03KRA03 250-500 mm	3.76	
03KRA03 250-500 mm	4.03	
03KRA03 250-500 mm Averag	*3.89*	*0.14*
03KRA03 125-250 mm	4.23	
03KRA03 125-250 mm	3.99	
03KRA03 125-250 mm	4.28	
03KRA03 125-250 mm	3.82	
03KRA03 125-250 mm	3.95	
03KRA03 125-250 mm Averag	*4.06*	*0.17*

[1]One standard deviation for all replicate measurements of the same size fraction

Table 2: U-series data for whole-rock samples and plagioclase separates

Sample	Ra (fg/g)	Ra(+/-), % 2s	Th (ppm)	U (ppm)	$^{230}Th/^{232}Th$ atomic	$(^{238}U)/(^{232}Th)$	$(^{230}Th)/(^{232}Th)$
03KRA01 WR	95.7	1.60	0.744	0.237	5.920E-06	0.968	1.097
03KRA01 GM	n.d.	n.d.	0.834	0.252	5.974E-06	0.918	1.107
03KRA01 Plag-large	n.d.	n.d.	0.056	0.009	5.883E-06	0.479	1.090
03KRA01 Plag-small (63-250 ㎜)	10.6	3.88	0.044	0.015	n.d.	1.004	n.d.
03KRA03 WR	74.4	1.58	0.580	0.167	5.913E-06	0.874	1.096
03KRA03 Plag-large (125-500+ ㎜)	7.1	4.21	0.054	0.009	5.900E-06	0.534	1.094
03KRA03 Plag-small (63-125 ㎜)	16.1	2.64	0.073	0.020	5.954E-06	0.845	1.104

Notes:

$(^{226}Ra)/[Ba]$ uses Ba concentration measured by ICP-MS (see supplementary information)

$(^{226}Ra)/(^{230}Th)$ and $(^{230}Th)/[Ba]$ for 01PL-small calculated assuming that $^{230}Th/^{232}Th$ was the

Errors on Th and U concentrations were better than 0.5% (2s) based on reproduciblity of roc

Errors (standard error of instrument runs) on Th isotopic composition were better than 1.05%

Reported uncertainty on Ra concentration measurements includes both in-run precision and t

(^{230}Th)/ (^{238}U)	(^{226}Ra)/ (^{230}Th)	(^{230}Th)/ [Ba] (dpy/mg)	(^{226}Ra)/ [Ba] (dpy/mg)
1.133	1.05	1202	1267
1.207	n.d.	1324	n.d.
2.279	n.d.	505	n.d.
n.d.	1.98	366	724
1.253	1.05	1294	1362
2.048	1.08	550	595
1.306	1.80	425	764

same as that in 01PL-large
‹ standards
› (2s)
he uncertainty in the concentration of 228Ra in the tracer solution (see Methods sectior